ABSTRACT

BAIK, SEUNGWON. Optimal Component Layout for Minimal Vulnerability of Weapon Systems. (Under the direction of Dr. Shu-Cherng Fang).

Vulnerability is one of the key features of weapon design. Lower vulnerability guarantees the survivability and sustainability of weapon systems on the battlefield. The weapon vulnerability is greatly affected by how the components are placed inside weapon systems. Yet, the optimal component layout problem has not been fully investigated due to its complexity. In this dissertation, a mathematical model for minimizing the vulnerability of weapon systems is proposed by utilizing a grid point approach. A mixed-integer nonlinear programming model is first formulated and converted to a mixed-integer linear programming problem using the concept of pseudo-Boolean expressions for computations. In addition, we propose a "zone-based restriction heuristic" method to generate solutions in a much more efficient manner. A practical instance and the analysis of numerical experiments are also provided to validate the proposed model and solution method.

Optimal Component Layout for Minimal Vulnerability of Weapon Systems

by
Seungwon Baik

A dissertation submitted to the Graduate Faculty of
North Carolina State University
in partial fulfillment of the
requirements for the Degree of
Doctor of Philosophy

Industrial Engineering

Raleigh, North Carolina
2021

APPROVED BY:

Dr. Yahya Fathi	Dr. Michael Kay
Dr. Osman Ozaltin	Dr. Shu-Cherng Fang Chair of Advisory Committee

DEDICATION

For my wife Nayoung and children, Soheon and Geonu.

BIOGRAPHY

Seungwon Baik was born and raised in Dae-gu, South Korea. He graduated from Korea Military Academy in 2008. He then studied at Seoul National University (Seoul, South Korea), where he received his Master's degree in Industrial Engineering under the supervision of Dr. S.-P. Hong in 2013. He joined the Department of Industrial and Systems Engineering at North Carolina State University (Raleigh, NC) in Fall 2017 to pursue his Ph.D. degree under the supervision of Dr. Shu-Cherng Fang.

ACKNOWLEDGEMENTS

During my Ph.D. study period at NCSU, I have received support and assistance from a significant number of people.

I would like to express my deepest appreciation to my advisor Dr. Shu-Cherng Fang. I first met him in the ISE/OR/MA 505 class in Fall 2017; his every word in class was crystal clear to me. His supervision and teaching have been consistently precise and correct to me until now. His guidance over the past three years always outlines a way forward whenever I face difficulties in my research. In particular, he was willing to spend his precious time leading me to the right way in preparing for my doctoral dissertation. I sincerely appreciate his effort and time and will remember his teaching and words in my whole life.

In Fall 2017, when my family came to the United States, we had difficulty adapting to the local area. During that time, there was beloved help from numerous people, especially those in the Korean community. It's hard for me to list each of them, but I would like to express my sincerest gratitude. Especially, Stan shared his precious time with me almost every week. The Mahanaim community always prayed and supported us during difficult times. Besides, many families always stayed with us like a big family of mine.

I would also like to thank my friends in the FANGroup and the ISE Department: Zheming Gao, Fengming Lin, Chi-Yi Chen, Jiang Shan, Qi An, Huihui Wang, Ling Zhang, Meijia Yang, Yang Dong, Nana Zhang, Ruotian Gao, Xuerui Gao, Linfeng Song, Chun-Han Wang, Srinivasan Balan, Amirreza Sahebi Fakhrabad, Rahman Khorramfar, Yunsoo Ha, and Sanghyun Choo. Moreover, I am very grateful to my committee members: Dr. Yahya Fathi, Dr. Michael Kay, and Dr. Osman Ozaltin, for their precious time and feedback to improve my research. Thanks to the graduate school representatives Dr. Mihn Tang and Dr. Min Liu for their kind support and help.

Lastly but not at least, I would like to express my gratitude and love to my wife and two children, who have always shared our joys and sorrows altogether. In particular, we had to go through the COVID-19 pandemic during my Ph.D. study period. Thankfully, everyone could endure well, yield to each other, and overcome the difficult time together. I also thank my parents and parents-in-law for always encouraging and supporting me no matter where I am.

TABLE OF CONTENTS

LIST OF TABLES

LIST OF FIGURES

CHAPTER

1

INTRODUCTION

1.1 Background

Weapons are used to win battles. There exist various factors that affect the performance of weapon systems. Firepower, mobility, and survivability can exemplify the performance characteristics of a ground weapon system. Among them, survivability is an essential feature for successful military operations. Since World War II, there have been discussions on the survivability of some well-known aircraft [Jab65; JC58]. The conceptual studies of weapon survivability started in the late 1960s [Arn69; Atk69]. Quite a few studies have been conducted to improve the survivability of weapon systems.

Weapon systems operate on battlefields with uncertainty. It is unpredictable to know when and how enemy threats attack a weapon system. As a common practice, the survivability of weapon systems is represented by a probability, denoted by P_S. The closer P_S is to 0, the less likely the weapon system is to survive. On the contrary, the closer P_S is to 1, the more likely the weapon system is to survive. The opposite concept of survivability is killability, which is also measured by the probability that the weapon system is killed [Bal03].

For a weapon system to be killed, the weapon system first has to be hit by an enemy threat. This probability depends on the proficiency of the crews and the avoiding capability of the weapon system. Once the weapon system is hit, the probability of being killed depends on the withstanding capability of the weapon system. Hence the killability of weapon systems can be represented by the two inabilities to avoid a known enemy's threat and to resist the enemy's threat. These two concepts are referred to as the susceptibility and the vulnerability of weapon systems, respectively. Hence the weapon killability and survivability can be characterized by the vulnerability and susceptibility of weapon systems.

Consequently, the survivability of a weapon system depends upon how well the weapon system can avoid and withstand enemy threats. Since the weapon vulnerability and susceptibility are independent concepts of each other, the survivability of weapon systems can be maximized when the vulnerability and susceptibility of weapon systems are minimized individually. Various techniques have been developed to reduce the susceptibility or vulnerability of weapon systems [Bal03; Dri13].

1.2 Motivation

The assessment of weapon vulnerability varies with the type of enemy threats [NRC93]. The vulnerable area (VA) approach is used as the primary assessment of the weapon's vulnerability. This approach measures vulnerability by the ratio of vulnerable areas to the entire area [Dri13]. The simulation software called COVART (Computation of Vulnerable Area and Repair Time) operates based on the VA approach [DSI], which is widely used to measure the vulnerability of weapon systems in the military field. It assumes a single hit with a recent upgrade to deal with various types of warheads [Bal03]. Through the COVART simulation software, we can analyze which component layout is more vulnerable. Given a limited number of component layouts, the COVART simulation computes each component layout's vulnerability and chooses the one with the lowest vulnerability. However, it is almost impossible to simulate all possible cases one by one to reach an optimal component layout using COVART software for a large size problem.

The vulnerability of weapon systems depends on how components are laid out inside the weapon system [Bal03; Dri13]. If we can flexibly assess weapon vulnerability, then we shall be able to formulate the problem as a mathematical optimization model. Moreover, if the mathematical model can be efficiently solved to reach an optimum layout for minimum vulnerability, then the shortcomings of the COVART program can be overcome.

There exists relatively little research in the current literature on building optimization models for minimum vulnerability because the VA approach computes weapon vulnerability based on the projected areas of each component under a hit from a given direction. These projected areas may overlap each other to form many irregular shapes that are hard to model in mathematical expressions. This motivates us to design a new approach for assessing vulnerability that allows us to formulate the problem in simple mathematical expressions.

1.3 Contribution

This dissertation proposes a new mathematical model for minimal weapon vulnerability of weapon systems, considering all component types and realistic constraints. We also propose a new approximated grid point (AGP) approach evolved from the existing VA approach to capture vulnerability in the proposed model. Based on the AGP approach, a mixed-integer nonlinear programming (MINLP) model is formulated first and converted into a mixed-integer linear programming (MILP) model using the concept of pseudo-Boolean expressions for finding exact optimal solutions. In addition, we provide a heuristic method to reduce the required computation for finding high-quality solutions in a much more efficient manner. The main contributions of this dissertation are tri-fold:

- We propose a new AGP approach to model the vulnerability of weapon systems. It approximates areas using grid points compared to the VA approach. The results converge as the density of the grid point set increases. In this way, we can keep the shape of the projected area without distortion. This approach enables us to realize the concept of weapon vulnerability into a mathematical model.
- With the AGP approach, we formulate an MINLP model including all component types and the concepts of partial penetration and redundant components. Then we design a linearization mechanism using the concept of pseudo-Boolean expressions for computational efficiency. This mechanism enables us to obtain optimal component layouts of weapon systems using commercial solvers.
- A zone-based restriction heuristic is proposed to generate high-quality solutions for a large scale component layout problem in a much faster manner.

1.4 Outline of Dissertation

This dissertation consists of three pieces of work. In the first piece of work, we propose a new approach for assessing weapon vulnerability that can be easily adopted in an optimization model. The second piece of work provides a mathematical model for finding the minimal vulnerability of weapon systems based on the proposed approach of assessment. In the third piece of work, we design a heuristic method to solve the proposed mathematical model in an efficient manner.

In Chapter 2, we review the literature on vulnerability of weapon systems. To discuss the vulnerability of weapon systems, the concepts of kill modes and components are introduced first, and then we explain how the kill modes and components are related to each other. We also present the vulnerability program, which is a commonly adopted procedure to analyze and reduce the weapon vulnerability in the military field. Then the literature on the optimal component layout problem is reviewed. We also briefly explore the well-known mixed-integer linear programming (MILP) problem based on which our proposed model is formulated.

Chapter 3 mainly explores the assessment approach for weapon vulnerability. As preliminaries, we introduce some basic concepts including threat directions, parallel projections, and geometry of cuboids in the 3-dimensional space. Then the commonly used VA approach is presented with simple examples. We also provide the proposed AGP approach and discuss the difference between the two approaches to show the advantages of using the proposed AGP approach.

Chapter 4 presents a mathematical model of the minimal vulnerability of weapon systems. We provide the problem statement and notations used for the proposed mathematical model, which includes all component types and realistic constraints for the feasibility in the 3D space, partial penetrations, and component redundancy. We formulate the problem as an MINLP model first and convert it to an MILP model by a linearization mechanism using the concept of pseudo-Boolean expressions.

Chapter 5 provides a heuristic method to solve the proposed MILP model. Although the proposed MILP model can be solved by using commercial solvers, we may undergo low computation efficiency caused by the large number of binary variables and constraints. The proposed heuristic method is designed by considering components' characteristics to improve computational efficiency through restricting the locations of some components. We present a practical instance to validate the proposed MILP model for optimal component layout using both of the commonly used Branch and Cut (B&C) method and the proposed

ZRH method. Then computational experiments are provided to analyze the performance of the proposed ZRH method with different sizes.

CHAPTER

2

LITERATURE REVIEW

This chapter reviews the literature on weapon vulnerability and optimal component layout problems. In Section 2.1, we introduce the basic concepts to define the vulnerability of weapon systems. The literature on the optimal component layout problem is investigated in Section 2.2. In Section 2.3, we present the mixed-integer linear programming (MILP) model to be used to formulate our mathematical model in this dissertation.

2.1 Basic Concepts

2.1.1 Survivability and Vulnerability

As mentioned in Section 1.1, the weapon survivability (P_S) represents the capability of weapon systems to be survived against the enemy's threats. The opposite concept of the weapon survivability is the weapon killability, denoted by P_K. Thus, the survivability and killability of weapon systems are mutually exclusive concepts and can be represented as the following [Bal03]:

$$\text{Survivability}\,(P_S) = 1 - \text{Killability}\,(P_K).$$

To assess the killability of weapon systems, we need to consider two sub-concepts: the inabilities to avoid enemy's threats and to withstand the enemy's threats. Using susceptibility, denoted by P_H, we can assess the inability of a weapon system to avoid the threat [Bal03]. Here the vulnerability, denoted by $P_{K/H}$, is defined as the inability of a weapon to withstand a man-made threat [Bal03; Dri13]. Hence the survivability and killability are characterized by the susceptibility (P_H) and vulnerability ($P_{K/H}$) as the following formulas [Bal03; Dri13]:

$$\text{Killability}\,(P_K) = \text{Susceptibility}\,(P_H) \cdot \text{Vulnerability}\,(P_{K/H}),$$
$$\text{Survivability}\,(P_S) = 1 - \text{Susceptibility}\,(P_H) \cdot \text{Vulnerability}\,(P_{K/H}).$$

Assuming a weapon system is hit by enemy's threats, i.e., the weapon susceptibility (P_H) is equal to one, then the survivability of the weapon system depends upon the weapon vulnerability only. Thus, the survivability of weapon systems subjected to a hit, denoted by $P_{S/H}$, can be represented as the following:

$$\text{Survivability given a hit}\,(P_{S/H}) = 1 - \text{Vulnerability}\,(P_{K/H}).$$

The vulnerability of weapon systems can also be considered as the conditional probability that the weapon system is disabled when it is hit. Both concepts of susceptibility and vulnerability are considered as probabilities in the range of $[0,1]$. The closer $P_{K/H}$ is to 1, the less likely the weapon system is to withstand the enemy's threat. On the contrary, the closer $P_{K/H}$ is to 0, the more likely the weapon system is to resist when it is hit. In short, the killability describes the inability of weapon systems to avoid and withstand enemy's threats. The susceptibility and vulnerability are independent concepts of each other. Many studies have been conducted in various fields to reduce the susceptibility and vulnerability of weapon systems [Bal94; Bal98; Har10; Hen82; Kol18; Mer16; Rem76; Wan19; Yi,14]. There exist at least 12 general concepts to improve the weapon survivability, i.e, to reduce the susceptibility or vulnerability, as shown in Table 2.1.

Notice that the survivability enhancement concepts are categorized by reducing either susceptibility or vulnerability. While the susceptibility reduction approaches are related to advanced science technologies, most vulnerability reduction approaches are linked to the components in a weapon system, such as component redundancy, location, shielding, elimination, or replacement. In other words, the vulnerability of weapon systems can be reduced by efficiently allocating various components inside the weapon system.

Table 2.1: The twelve survivability enhancement concepts [Bal03].

Susceptibility(P_H) reduction	Vulnerability($P_{K/H}$) reduction
Threat warning	Component redundancy (with separation)
Noise jamming and deceiving	Component location
Signature reduction	Passive damage suppression
Expendables	Active damage suppression
Threat suppression	Component shielding
Weapon and tactics, flight performance and crew training and proficiency	Component elimination or replacement

2.1.2 Kill Modes and Components

Weapon systems continue to perform some essential combat functions on the battlefield. Ground weapon systems, such as armored vehicles, basically have mobility and firepower as combat functions. The combat functions may be inevitably disabled by the damage from the enemy's threats. The damages inflicted on weapon systems cause some disabilities of major combat functions, and these disabilities of the major combat functions are called kill modes.

Kill modes are defined as the specific natures of damage inflicted on the target [Dri13]. Phrases such as damage definition, damage criterion, kill levels or kill criteria are used as synonyms [Dri13; Bal03]. Kill modes refer to a state that a specified primary combat function does not operate properly. For ground vehicles, examples of kill modes are provided as follows [Dri13]:

- K-catastrophic kill (not repairable),
- M0-mobility kill (cannot move, immediately),
- M40-mobility kill (cannot move within 40 min),
- F-firepower kill (cannot fire).

The K-catastrophic kill (K-kill) indicates that the weapon system is completely destroyed, no longer operating, and is not repairable. The M0-mobility kill (M-kill) refers to a state in which the drive of the weapon system is no longer possible. F-firepower kill (F-kill) notes a state in which firepower such as machine guns are no longer functional [Dri13].

If necessary, we can subdivide some kill modes into more detailed criteria based on the analysis purpose. For example, M40-mobility kill (M-kill for 40 min) can be used to describe the status that weapon systems cannot move within 40 minutes due to the damage inflicted on the weapon systems.

The components inside weapon systems have their roles or functions. In terms of an entire weapon system, the weapon system operates properly when the components work correctly. Some components affect the kill modes, and other components may not. For example, a cooler system for crews in land vehicles does not affect any kill modes, such as M-kill and F-kill. The cooling system is necessary to provide crew comfort but does not cause any disability of main combat functions. Thus, we can categorize each component depending on whether the component is related to the kill modes. Typically, a component in a weapon system can be categorized as below.

- critical component(without redundancy or with redundancy),
- redundant component,
- non-critical component.

Critical components are the components that directly affect one or more kill modes of a weapon system [Bal03; Dri13]. For example, if the wheels of a ground weapons system become disabled, M-kill naturally occurs. Some critical components may have a spare component in the weapon system. The spare components are called redundant components. A pair of critical and its corresponding redundant component is connected to the same combat function. Hence only when both the critical and its corresponding redundant components get disabled, the failure of the corresponding combat function actually occurs. Non-critical components do not affect any kill modes when they are destroyed. However, we need to include the non-critical components in our mathematical model because they may protect critical components behind them. Figure 2.1 illustrates the relations of kill modes and components types using the fault tree.

In Figure 2.1, the fault tree contains six components and two kill modes. If component 1 becomes disabled, M-kill occurs because the component 1 is connected to M-kill with the OR gate. Component 2 has a link with both M-kill and F-kill in the fault tree. This means the failure of the component 2 causes both kill modes: M-kill and F-kill. Besides, the components 1 and 2 do not have any spare components as backups. Hence the components 1 and 2 are called critical components without redundancy. F-kill is affected by not only

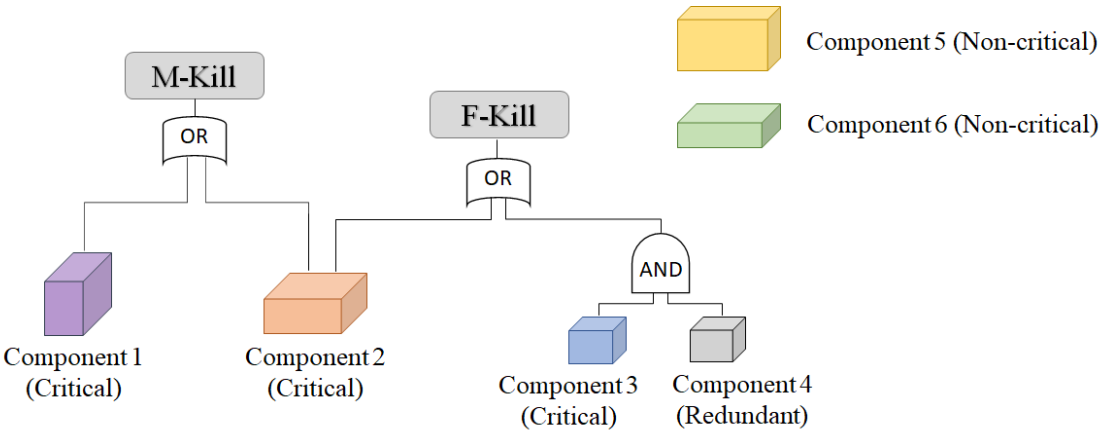

Figure 2.1: Fault tree.

the component 2 but also components 3 and 4. If the component 2 is intact, F-kill occurs only when both the components 3 and 4 are disabled by the AND gate. Hence one of the components 3 and 4 is a critical component with redundancy, and the other is called its corresponding redundant component. Components 5 and 6 are not connected to any kill modes in the fault tree. Thus, they are called non-critical components. These non-critical components do not affect any kill modes. However, it is necessary to include the non-critical components in mathematical models for considering partial penetrations and 3D feasibility of components. The proposed mathematical optimization model in this dissertation considers all types of components: critical (with redundancy), critical (without redundancy), redundant, and non-critical components.

This dissertation defines components as interrelating entities inside a weapon system, such as an engine, a generator, and a gas tank. We can break down the components into lower-level parts according to the analysis purpose [Dri13].

2.1.3 The Vulnerability Program

There is a typical procedure in the military field to analyze the vulnerability weapon systems, called the vulnerability program. The following procedures are generally carried out to assess and reduce the vulnerability of weapon systems in practice [Bal03].

- Task 1: Identify the critical components and their kill modes
  (What makes the weapon system vulnerable?)
- Task 2: Perform a vulnerability assessment (How vulnerable is the weapon system?)

- Task 3: Design for low vulnerability using vulnerability reduction technology

The objective of Task 1 is to determine kill modes and identify critical components of weapon systems. Task 1 clarifies which components cause the defined kill modes. As shown in Figure 2.1, fault trees can present the relations between critical components and kill modes. As a result of Task 1, we may acquire fault trees to clarify the relations of the kill modes and components. This task enables us to recognize which components make the weapon system vulnerable. In this dissertation, it is assumed that the defined kill modes and the related critical components are provided.

Task 2 is the process to specify the enemy's threat and decide the assessment approach for the vulnerability analysis. The assessment of vulnerability varies with the threat type [NRC93]. The enemy's threats to weapon systems vary from a non-explosive penetrating warhead to a high-explosive incendiary. Hence, we need to apply different types of analysis approaches to assess weapon systems' vulnerability depending on the type of enemy's threats. In this task, the enemy threat is first assumed as one type, such as a non-explosive penetrating warhead, and an adequate assessment approach is determined accordingly. In this dissertation, we assume that the enemy's threat is a non-explosive penetrating warhead, and adopt a new vulnerability assessment approach developed from the existing assessment approach.

Task 3 is to design weapons systems with lower vulnerability using vulnerability reduction technologies. As discussed in Subsection 2.1.1, the concept of vulnerability reduction is summarized into six approaches: component redundancy, component location, passive damage suppression, active damage suppression, component shielding, and component elimination or replacement. Most of these technologies use component layouts inside weapon systems. The component-related reduction technologies are relatively cost-saving tasks, such as efficiently placing components or adding spare components. In our dissertation, we present a mathematical model of the optimal component layout for the minimal vulnerability of weapon systems. We expect not only that this proposed model can provide the optimal component layout for a given component set, but also provide meaningful information on component redundancy and component elimination.

The research scope in this dissertation is directly relevant to Tasks 2 and 3. In the vulnerability program, the weapon vulnerability is assessed in Task 2, and some technologies are applied to reduce the weapon vulnerability in Task 3. We propose a new assessment approach called the grid point approximation approach in Chapter 3, and formulate an optimization model achieving the minimal vulnerability of weapon systems in Chapter 4.

2.2 Literature of Optimal Component Layout of Weapon Systems

The vulnerable area (VA) approach is used as the primary assessment of the weapon vulnerability [Bal03]. This approach measures vulnerability by the ratio of vulnerable areas to the entire area. The vulnerable area is defined as the product of the critical components' presented areas and the corresponding kill probabilities [Dri13]. We will explain the concept of the VA approach in more details in Chapter 3. As mentioned in Section 1.2, the simulation software called COVART (Computation of Vulnerable Area and Repair Time) is widely used to measure the vulnerability of weapon systems based on the VA approach. Given a limited number of component layouts, COVART can compute the vulnerability of each layout and choose the one with the lowest vulnerability. However, if component layouts are relatively flexible and we want to find an optimal layout involving many components, it is hard to expect the simulation software covers all the possible combinations for considerations in a time limit.

Recently, studies using mathematical models have been proposed to overcome the limitation of the COVART software. A mixed-integer linear programming (MILP) model was proposed for the minimal weapon vulnerability [Jee18; Jee19]. The studies in [Jee18; Jee19] consider critical and redundant components only. However, in reality, non-critical components are also essential for the optimal layout because they play a crucial role in dealing with partial penetration. For obtaining the feasible component layout inside weapon systems, non-critical components also need to be included in mathematical models. In addition, the studies in [Jee18; Jee19] use squares to approximate the projected areas of components for adopting the VA approach.

Figure 2.2 presents a layout of two components 1 and 2 with their centroids c_1 and c_2. The two projected components have an overlap area, which affects the calculation of the weapon vulnerability. With the same centroids c_1 and c_2, the two projected areas are converted into squares. Even though the converted squares have the same areas as the original projected areas, the overlap area may be ignored as shown in Figure 2.2. Thus, the approach in [Jee18; Jee19] enables us to obtain projected areas simply, but may provide relatively inaccurate overlap areas. Based on this vulnerability assessment approach, a mixed-integer linear programming (MILP) model is formulated using approximated squares in [Jee18; Jee19].

Other than the study in [Jee18; Jee19], related component layout issues on satellites

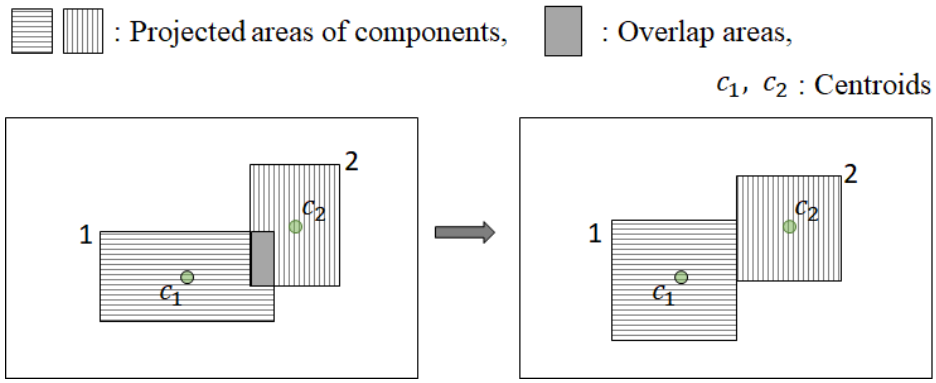

Figure 2.2: Projected areas approximated by squares.

can be referred to [Qin17; Qin18; Zho19] using different calculation mechanisms from the vulnerability of weapon systems.

2.3 Mixed Integer Linear Programming

The proposed mathematical model in this dissertation is formulated as a mixed-integer nonlinear programming (MINLP) model first, and converted into a mixed-integer linear programming (MILP) model using the concept of pseudo-Boolean expressions for computations. The MILP model with binary variables can be represented by the followings:

$$\begin{aligned} \min \quad & \mathbf{c}^T\mathbf{x} + \mathbf{d}^T\mathbf{z} \\ \text{s.t.} \quad & A\mathbf{x} + B\mathbf{z} \le \mathbf{b}, \\ & \mathbf{x} \ge 0, \ \ \mathbf{z} \in \{0,1\}^p, \end{aligned} \tag{2.1}$$

where $\mathbf{x}\,(\in \mathbf{R}^n)$: a vector of n continuous variables,
$\mathbf{z}\,(\in \{0,1\}^p)$: a vector of p binary variables,
$\mathbf{c}, \mathbf{d}$: $(n \times 1)$ and $(p \times 1)$ vectors of parameters,
A, B : $(m \times n)$ and $(m \times p)$ matrices,
$\mathbf{b}$: a $(m \times 1)$ vector.

The above MILP system includes continuous variables $\mathbf{x} \in (\mathbf{R}^n)$ and binary variable $\mathbf{z}\,(\in \{0,1\}^p)$. All the constraints are in linear forms with binary integer or continuous variables. In this section, we briefly discuss the complexity issue in the MILP model and its algorithms.

The MILP problem with binary variables can be solved by enumerating all possible

combinations of the binary variable $\mathbf{z}$ ($\in \{0,1\}^p$). This requires that we solve 2^p linear programming (LP) problems [Flo95; D'A17]. This may demand an enormous amount of time to solve. Besides, the MILP problem is known to be a problem belonging to the class of *NP*-complete problems [Vav91]. Several approaches have been proposed to improve the computation efficiency as follows [Flo95; Wol98]:

- branch and bound method,
- cutting plane algorithms: valid inequalities and Gomory's fractional cutting plane algorithms,
- decomposition algorithms: variable partitioning, duality, and relaxation methods,
- column generation algorithms: Dantzig-Wolfe reformulation, solving the master linear program and integer programming (IP) column generation,
- heuristic methods: greedy local search and improved local search heuristics: tabu search, simulated Annealing and genetic algorithms.

In this dissertation, the optimal component layout problem is formulated by an MINLP model first, then linearized into a MILP model using the concept of pseudo-Boolean expressions. The proposed MILP model enables us to find optimal solutions using any commercial software. Some readily available MILP solvers include ILOG CPLEX [ILO], Gurobi, LINDO, Mosek, XPRESS-MP [Lin11] and AMPL [Ji 19]. We solve the proposed MILP model using CPLEX using the Branch and Cut (B&C) algorithm, which involves a branch and bound algorithm with cutting planes [Lin11; Wol98; Wan19]. Then we propose a "zone-based restriction" heuristic method to overcome low efficiency caused by a large number of variables and constraints in Chapter 5.

CHAPTER

3

VULNERABILITY ASSESSMENTS OF WEAPON SYSTEMS

In this chapter, we study on the vulnerability assessments of weapon systems. In Section 3.1, some basic concepts and observations are provided to measure the weapon vulnerability. In Section 3.2, we introduce the vulnerable area (VA) approach, which is widely used to assess the vulnerability of weapon systems. The new approximated grid point (AGP) approach is proposed to adopt the concept of the weapon vulnerability in optimization models in Section 3.3.

3.1 Preliminaries

In this section, we investigate some basic concepts to assess the vulnerability of weapon systems.

3.1.1 Threat Directions

Enemy threats may be of various types: non-physical forms such as electronic attacks or non-explosive penetrating warheads. In this dissertation, it is assumed that the enemy threats are non-explosive warheads causing penetration on weapon systems. Threat directions (θ, ϕ) are defined as the horizontal (θ) and vertical (ϕ) angles of the warheads toward weapon systems in the 3-dimensional (3D) space [Bal03; Dri13].

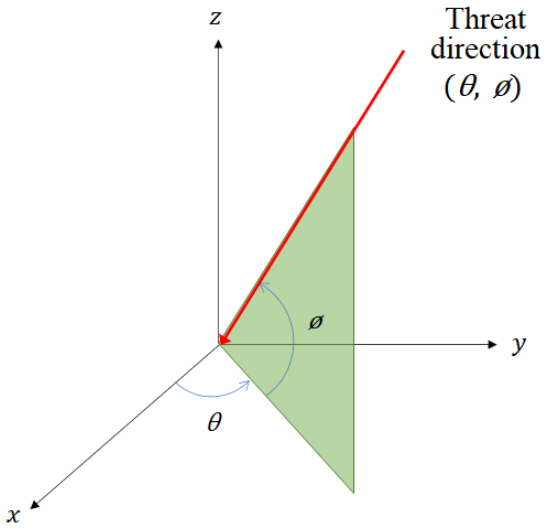

where $\theta \in [0°, 360°)$ and $\phi \in [-90°, 90°]$.

Figure 3.1: Threat directions (θ, ϕ).

As shown in Figure 3.1, the horizontal (θ) angle increases counterclockwise starting from the direction of $+x$ axis in the range of $[0°, 360°)$. The vertical angle (ϕ) increases toward the $+z$ axis, and decreases to the $-z$ axis from the $x-y$ plane in the 3D space in the range of $[-90°, 90°]$. Then we can represent every threat direction toward weapon systems by using the horizontal $(\theta \in [0°, 360°))$ and vertical $(\phi \in [-90°, 90°])$ angles. The threat directions can be also considered as a 3D vector $(-\cos\theta, -\sin\theta, -\tan\phi)^T$ [Jee18].

3.1.2 Parallel 2D Transformation from the 3D Space

The vulnerability of weapon systems can be assessed from a known threat direction (θ, ϕ). To compute the vulnerability from the known threat direction (θ, ϕ), we need to project the exterior hull of a weapon system and the components inside the weapon system to 2-dimensional (2D) space. The detailed approaches for vulnerability computations are discussed in Sections 3.2 and 3.3. This subsection briefly describes the transformation of axes and the projection from the 3D space to the 2D space.

In this dissertation,it is assumed that the exterior hull and components of weapon systems are cuboid-shaped, and they are located in $\mathbb{R}^3_+$. Let L, W, and H be the length, width, and height of the exterior hull, respectively. Then we suppose one of the two bottom left vertices of the exterior hull is placed at the origin $O(0,0,0)^T$ in the 3D space. In other words, we assume that the range of exterior hulls is $([0, L], [0, W], [0, H])$, as shown in Figure 3.2.

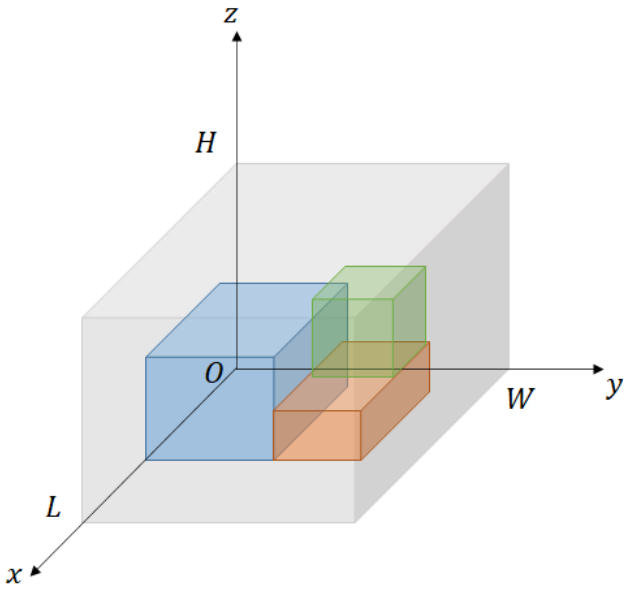

Figure 3.2: Exterior hull and components in the 3D space.

The 2D transformation from the 3D space was investigated in [Jee18]. With a known a threat direction (θ, ϕ), the origin $O(0,0,0)^T$ in the 3D space is projected to the new origin $O'(0,0)^T$ in the 2D space, as shown in Figure 3.3. Using the known threat direction (θ, ϕ),

two vectors $\mathbf{x}_{(\theta,\phi)}$ and $\mathbf{y}_{(\theta,\phi)}$ are generated by Eqs. (3.1) and (3.2), which are orthogonal to each other. Then the projected 2D plane $\mathbf{x}_{(\theta,\phi)} - \mathbf{y}_{(\theta,\phi)}$ is composed of these two vectors $\mathbf{x}_{(\theta,\phi)}$ and $\mathbf{y}_{(\theta,\phi)}$ [Jee18].

$$\mathbf{x}_{(\theta,\phi)} = (\sin\theta, -\cos\theta, 0)^T \tag{3.1}$$

$$\mathbf{y}_{(\theta,\phi)} = \left(\frac{-\cos\theta\tan\phi}{\sqrt{1+\tan^2\phi}}, \frac{-\sin\theta\tan\phi}{\sqrt{1+\tan^2\phi}}, \frac{1}{\sqrt{1+\tan^2\phi}}\right) \tag{3.2}$$

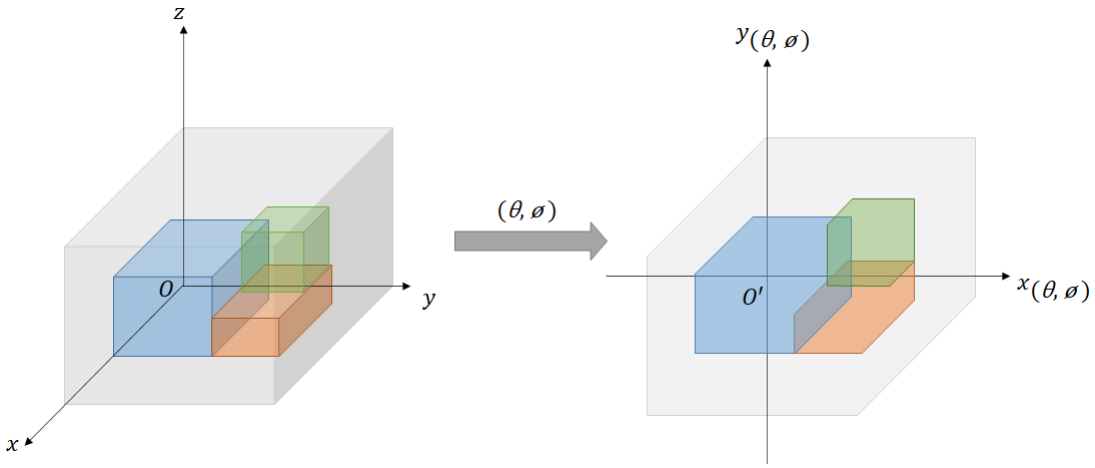

Figure 3.3: 2D transformation from the 3D space.

With a known threat direction (θ, ϕ), any point $(x, y, z)^T$ in the 3D space can be projected to the point $(x^{(\theta,\phi)}, y^{(\theta,\phi)})^T$ in the 2D plane $\mathbf{x}_{(\theta,\phi)} - \mathbf{y}_{(\theta,\phi)}$ as the following [Jee18]:

$$\begin{bmatrix} \bar{x} \\ \bar{y} \end{bmatrix} = \Lambda \begin{bmatrix} x \\ y \\ z \end{bmatrix} = \begin{bmatrix} \sin\theta & -\cos\theta & 0 \\ \frac{-\cos\theta\tan\phi}{\sqrt{1+\tan^2\phi}} & \frac{-\sin\theta\tan\phi}{\sqrt{1+\tan^2\phi}} & \frac{1}{\sqrt{1+\tan^2\phi}} \end{bmatrix} \begin{bmatrix} x \\ y \\ z \end{bmatrix}. \tag{3.3}$$

Consequently, by using Eqs.(3.1), (3.2), and (3.3), the exterior hull and components in a weapon system can be projected to the 2D space with the new origin $O'(0,0)^T$, as shown in Figure 3.3.

3.1.3 2D Projection of Cuboids

As mentioned in Subsection 3.1.2, the exterior hull and components inside weapon systems are assumed to be cuboid-shaped. In this subsection, we provide some useful observations of the geometry of cuboids to formulate our mathematical model in Chapter 4.

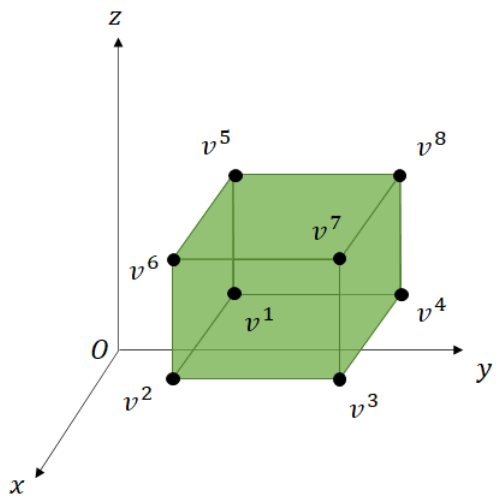

Figure 3.4: Indexed vertices of cuboids.

Cuboids have 8 vertices. The indices from one to eight are assigned to the vertices of cuboids based on their locations, as shown in Figure 3.4. For example, the front top right vertex is denoted by v^7. When we project a cuboid to the 2D space, only a few vertices of the cuboid are used to form the projected polygon in the 2D space. In Figure 3.4, if we have a threat direction of (θ, ϕ) in the range of $((0°, 90°), (0°, 90°))$, the projected polygon is composed of the vertices $v^5, v^8, v^4, v^3, v^2, v^6$. In this way, using the indexed vertices, we can identify which vertices of cuboids form the polygons in the 2D space. We present every case depending on the known threat directions (θ, ϕ) as follows:

- Case 1 : $(v^2, v^3, v^4, v^5, v^6, v^8)$ for $\theta_1 = (0°, 90°)$ and $\phi_1 = (0°, 90°)$,
- Case 2 : $(v^1, v^3, v^4, v^5, v^6, v^7)$ for $\theta_2 = (90°, 180°)$ and $\phi_2 = (0°, 90°)$,
- Case 3 : $(v^1, v^2, v^4, v^6, v^7, v^8)$ for $\theta_3 = (180°, 270°)$ and $\phi_3 = (0°, 90°)$,
- Case 4 : $(v^1, v^2, v^3, v^5, v^7, v^8)$ for $\theta_4 = (270°, 360°)$ and $\phi_4 = (0°, 90°)$,

- Case 5 : $(v^1, v^3, v^4, v^5, v^6, v^7)$ for $\theta_5 = (270°, 360°)$ and $\phi_5 = (-90°, 0°)$,
- Case 6 : $(v^2, v^3, v^4, v^5, v^6, v^8)$ for $\theta_6 = (180°, 270°)$ and $\phi_6 = (-90°, 0°)$,
- Case 7 : $(v^1, v^2, v^3, v^5, v^7, v^8)$ for $\theta_7 = (90°, 180°)$ and $\phi_7 = (-90°, 0°)$,
- Case 8 : $(v^1, v^2, v^4, v^6, v^7, v^8)$ for $\theta_8 = (0°, 90°)$ and $\phi_8 = (-90°, 0°)$,
- Case 9 : (v^2, v^3, v^6, v^7) or (v^1, v^4, v^5, v^8) for $(\theta_9, \phi_9) = (0°, 0°)$ or $(180°, 0°)$,
- Case 10 : (v^1, v^2, v^5, v^6) or (v^3, v^4, v^7, v^8) for $(\theta_{10}, \phi_{10}) = (90°, 0°)$ or $(270°, 0°)$,
- Case 11 : (v^1, v^2, v^3, v^4) or (v^5, v^6, v^7, v^8) for $(\theta_{11}, \phi_{11}) \in ([0°, 360°), 90°)$ or $([0°, 360°), -90°)$,
- Case 12 : (v^2, v^3, v^5, v^8) for $(\theta_{12}, \phi_{12}) \in (0°, (0°, 90°))$ or $(180°, (-90°, 0°))$,
- Case 13 : (v^1, v^4, v^6, v^7) for $(\theta_{13}, \phi_{13}) \in (0°, (-90°, 0°))$ or $(180°, (0°, 90°))$,
- Case 14 : (v^3, v^4, v^5, v^6) for $(\theta_{14}, \phi_{14}) \in (90°, (0°, 90°))$ or $(270°, (-90°, 0°))$,
- Case 15 : (v^1, v^2, v^7, v^8) for $(\theta_{15}, \phi_{15}) \in (90°, (-90°, 0°))$ or $(270°, (0°, 90°))$.

As presented above, unless both of horizontal (θ) and vertical (ϕ) angles are parallel to any axes, six vertices out of 8 are used to be the vertices of the projected polygon in the 2D space. If any angle is parallel to any axes ($\theta = 90°n, n = 0, 1, 2, 3, \phi = 90°m, m = -1, 0, 1$), only four vertices are required. Hence cuboids are projected to hexagons or a quadrilaterals in the 2D space, as presented in Cases $1-8$ or $9-15$, respectively. Figure 3.5 illustrates examples for Cases 1 and 10. The projected vertices by the threat direction (θ_i, ϕ_i) are denoted by $v^k_{(\theta_i,\phi_i)}$, $k = 1, 2, ..., 8$, which can can be obtained by Eq.(3.3).

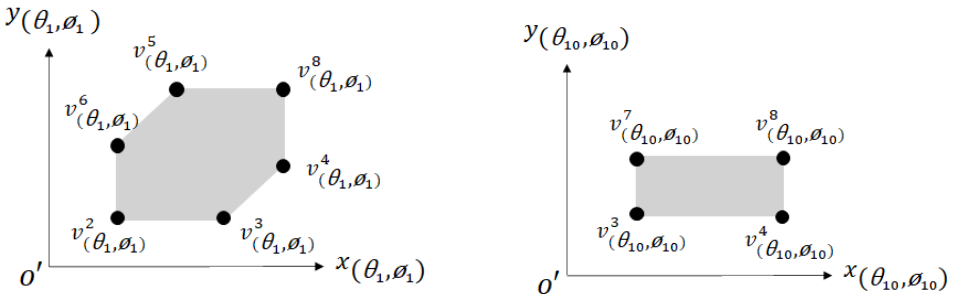

(a) Case 1 (b) Case 10

Figure 3.5: Polygons projected from cuboids.

In this way, we can identify four or six vertices of the original cuboids to compose a projected polygon in the 2D space based on the known threat direction (θ, ϕ). In other words, cuboids in the 3D space are projected to quadrilaterals or hexagons to the 2D space, which can be represented by four or six linear inequalities. Figure 3.6 present a linear inequality $(\mathbf{a}_m)^T\mathbf{x} \geq e_m, m = 1, 2, ..., 4(\text{or } 6)$ enclosing an edge of the projected hexagon, where $\mathbf{a}_m$ is the normal vector and e_m is the intercept.

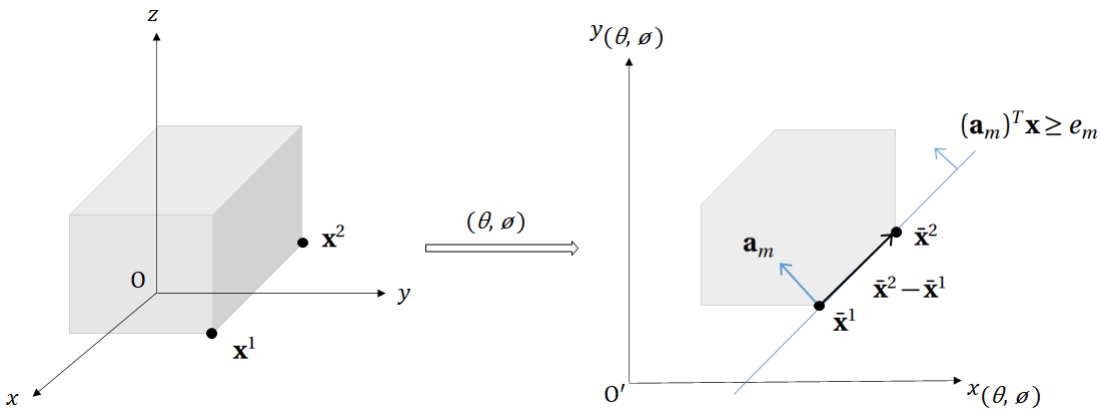

Figure 3.6: Normal vector representing an edge of the projected area.

In Figure 3.6, from a known threat direction (θ, ϕ), two vertices $\mathbf{x}^1$ and $\mathbf{x}^2$ of the cuboid are projected to two points $\bar{\mathbf{x}}^1$ and $\bar{\mathbf{x}}^2$ in the 2D space. The linear inequality $\mathbf{a}_m^T\mathbf{x} \geq e_m$ shown in Figure 3.6 includes the vector $\bar{\mathbf{x}}^2 - \bar{\mathbf{x}}^1$ on the boundary. The normal vector $\mathbf{a}_m$ and the vector $\bar{\mathbf{x}}^2 - \bar{\mathbf{x}}^1$ are orthogonal, i.e., $(\mathbf{a}_m)^T(\bar{\mathbf{x}}^2 - \bar{\mathbf{x}}^1) = 0$. Here the vector $\bar{\mathbf{x}}^2 - \bar{\mathbf{x}}^1$ in Figure 3.6 can be represented by $\bar{\mathbf{x}}^2 - \bar{\mathbf{x}}^1 = \Lambda(\mathbf{x}^2 - \mathbf{x}^1)$ as shown in Eq.(3.3). Thus, the normal vector $\mathbf{a}_m$ is dependent on the threat direction (θ, ϕ) and the known vertices $\mathbf{x}^1$ and $\mathbf{x}^2$ of the cuboid. In other words, the normal vector $\mathbf{a}_m$ is independent of the location of cuboids.

The intercept e_m of the linear inequality can be represented $e_m = (\mathbf{a}_m)^T\bar{\mathbf{x}}^1 = (\mathbf{a}_m)^T\Lambda\mathbf{x}^1$ since the point $\bar{\mathbf{x}}^1$ is on the boundary of the linear inequality $\mathbf{a}_m^T\mathbf{x} \geq e_m$. Thus the intercept e_m is dependent on the transition matrix Λ and the 3D coordinate $\mathbf{x}^1 (\in \mathbf{R}^3_{++})$. Since the transition matrix Λ is represented by the known threat direction (θ, ϕ), so the intercept e_m depends on the location of cuboids. In other words, the intercept e_m can be represented by the linear combinations of the centroid of cuboids.

3.2 Vulnerable Area Approach and its Complexity Issue

In this section, we introduce vulnerable area approach which is widely used to assess the vulnerability of weapon systems [Bal03; Dri13]. We also review a limitation of the approach to be adopted in mathematical models.

3.2.1 Vulnerable Area Approach

The vulnerable area (VA) approach is commonly used to assess the weapon vulnerability. The approach is straightforward and simple to apply for a given component layout. Besides, it is known that the simulation software, called COVART (Computation of Vulnerable Area and Repair Time), operates based on the VA approach to assess the vulnerability of weapon systems [Dri13].The VA approach defines vulnerability as the ratio of summation of vulnerable areas to an entire area. With a known threat direction (θ, ϕ), the weapon vulnerability is calculated by the following formula [Bal03; Dri13]:

$$v(\theta,\phi) = \frac{\Sigma_i \{A_i(\theta,\phi) \times p_i\}}{A_0(\theta,\phi)}, \tag{3.4}$$

where (θ, ϕ) : horizontal (θ) and vertical (ϕ) angles of a known threat direction,
$v(\theta,\phi)$: vulnerability of a weapon system from the threat direction (θ,ϕ),
$A_i(\theta,\phi)$: the projected area of component i from the threat direction (θ,ϕ),
p_i : the probability of failure of component i given a hit on component i,
$A_0(\theta,\phi)$: the projected area of the entire weapon system from the threat direction (θ,ϕ).

In Eq. (3.4), the term $A_i(\theta,\phi) \times p_i$ indicates the vulnerable area of component i. Every component in the 3D space is projected to the 2D space using the known threat direction (θ,ϕ) to obtain the projected areas. We provide examples to show the calculation of the VA approach in Figures 3.7 and 3.8.

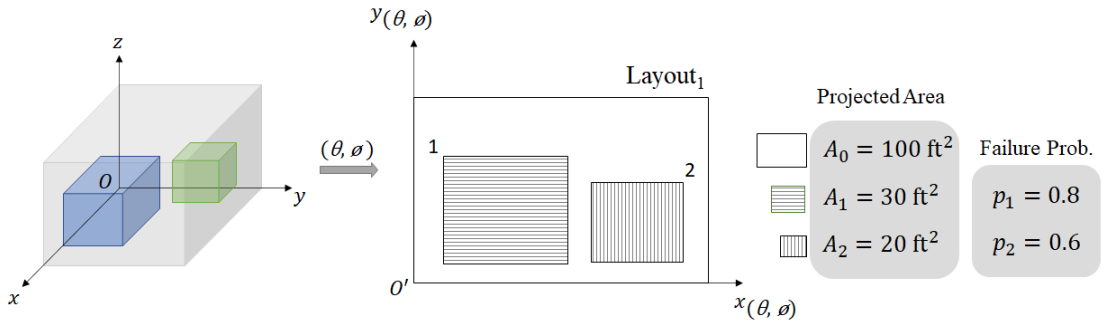

Figure 3.7: Example of the vulnerable area approach with non-overlap areas.

Figure 3.7 presents a layout of two components 1 and 2 without any overlaps. The projected areas (A_0, A_1, A_2) and failure probabilities (p_1, p_2) are given in Figure 3.7. Using Eq. (3.4), the vulnerability can be calculated as the following:

$$v(\theta,\phi) = \frac{\Sigma_i\{A_i(\theta,\phi)\times p_i\}}{A_0(\theta,\phi)} = \frac{A_1(\theta,\phi)\times p_1 + A_2(\theta,\phi)\times p_2}{A_0(\theta,\phi)} = \frac{30(0.8)+20(0.6)}{100} = 0.36.$$

The result indicates that the weapon vulnerability from the known direction (θ,ϕ) is 0.36. If we have any overlap areas, it is necessary to to obtain overlap and non-overlap areas separately. Additional example including an overlap area is provided in Figure 3.8.

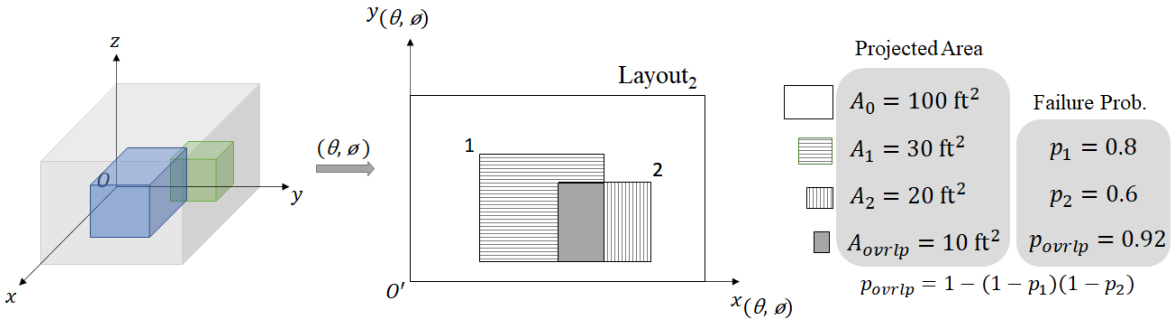

Figure 3.8: Example of the vulnerable area approach with overlap areas.

In Figure 3.8, there exist one overlap area and two non-overlap areas. The failure probability of the overlap area (p_{ovrlp}) can be represented by $p_{ovrlp} = 1-\{(1-p_1)(1-p_2)\}$. Then we can calculate the vulnerability by using Eq. (3.4) as the following:

$$\begin{aligned} v(\theta,\phi) &= \frac{\Sigma_i\{A_i(\theta,\phi)\times p_i\}}{A_0(\theta,\phi)} \\ &= \frac{\{A_1(\theta,\phi)-A_{ovrlp}\}\times p_1+\{A_2(\theta,\phi)-A_{ovrlp}\}\times p_2+A_{ovrlp}(\theta,\phi)\times p_{ovrlp}}{A_0(\theta,\phi)} \\ &= \frac{(30-10)(0.8)+(20-10)(0.6)+10(0.92)}{100} = 0.312. \end{aligned}$$

With the overlap area in Figure 3.8, we obtained the weapon vulnerability of the given component layout from the know threat direction (θ,ϕ). Compared to the previous example in Figure 3.7, the weapon vulnerability is decreased from 0.360 to 0.312 because of the overlap area. The above two examples imply that the VA approach requires the exact overlap areas to calculate vulnerability of weapon systems. Moreover, we can observe that the vulnerability with a known threat direction may be decreased if components are overlapped properly. Once the vulnerabilities are assessed from multiple threat directions, we may take a simple mean or weighted-sum of the vulnerabilities to determine the vulnerability of the entire weapon system [Jee18].

3.2.2 Complexity Issue of Overlap Area Calculation

In this subsection, we point out the complexity issue of the VA approach to be adopted in mathematical models. As we discussed in Subsection 3.2.1, the VA approach calculates the vulnerability of weapon systems based on vulnerable areas, defined as the product of projected areas and the corresponding failure probabilities. When we project a component layout of weapon systems, some components may be overlapped from a known threat direction. Hence we have to obtain all overlap areas to calculate the vulnerability of a weapon system to use the VA approach. If the overlap areas are presented as irregular polygons shown in Figure 3.9, it becomes complicated to compute the vulnerability.

In Figure 3.9, three components are placed inside the exterior hull, and the components are projected to the 2D space. Even though we consider only three components with

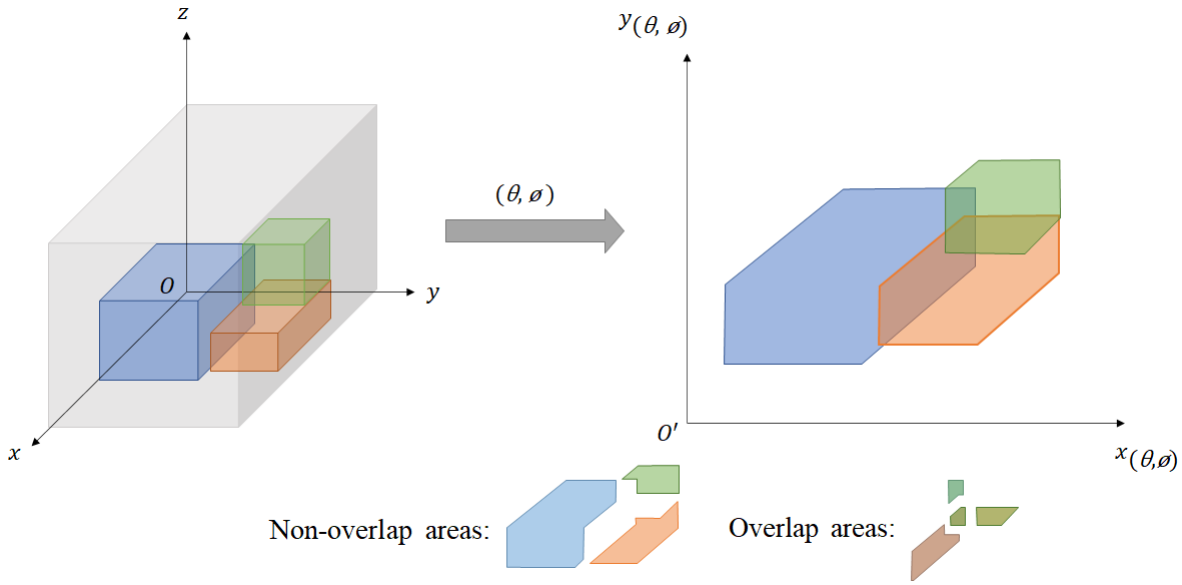

Figure 3.9: Non-convex or overlap areas in the vulnerable area approach.

overlaps, seven different shaped areas are generated by the overlaps. Most of them are complicated non-convex shapes shown in Figure 3.9. Even for a convex shape, we need to identify the coordinates of the vertices individually to calculate their exact area. It may be mathematically possible to get all the areas exactly, but it may be inefficient in computation complexity. Hence we propose a new approximated grid approach to measure vulnerability in the next section.

3.3 Approximated Grid Point Approach

In this section, we propose a new approximation approach using grid points to capture the vulnerability of weapon systems. The approximated grid point (AGP) approach is characterized by its use of grid points rather than areas. The grid points are generated to cover the projected exterior hull of weapon systems, as shown in Figure 3.10. The density of grid points can be adapted for the analysis purpose.

As shown in Figure 3.10, we can identify which projected component includes each grid point. For grid point k presented in Figure 3.10, we can define set S_k as the component set that includes the grid point k. For example, the projected areas of components 1 and 2 include the grid point k in Figure 3.10, so we have the set $S_k = \{1,2\}$. Thus, the failure probability at grid point k can be represented by $\pi_k = 1 - \prod_{i \in S_k}(1-p_i)$, where p_i denotes

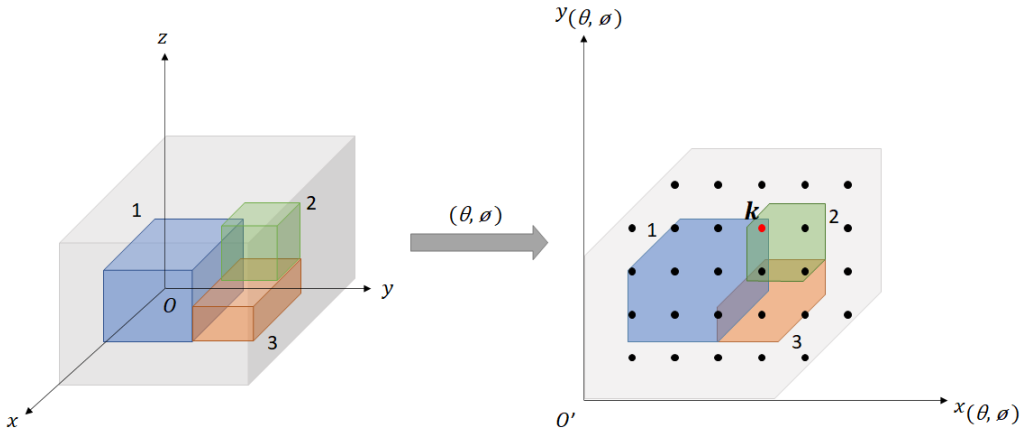

Figure 3.10: Grid points for the approximated grip point approach.

the failure probability of component i. Then the vulnerability of weapon systems with a known threat direction (θ,ϕ) is defined as the following:

$$v(\theta,\phi)=\frac{\Sigma_{k\in G_{(\theta,\phi)}}\pi_k}{|G_{(\theta,\phi)}|}, \tag{3.5}$$

where (θ,ϕ): horizontal (θ) and vertical (ϕ) angles of a known threat direction,
$v(\theta,\phi)$: vulnerability of a weapon system given the threat direction (θ,ϕ),
π_k: the failure probability at the k^{th} grid point,
$G_{(\theta,\phi)}$: the set of grid points covering the projected exterior hull from the threat direction (θ,ϕ),
$|G_{(\theta,\phi)}|$: the number of grid points in $G_{(\theta,\phi)}$.

The weapon vulnerability from a known threat direction $v(\theta,\phi)$ can be calculated by Eq. (3.5). Assuming that a single hit occurs uniformly distributed at each grid point, the weapon vulnerability $(P_{K/H})$ can be defined as $P_{K/H}\triangleq\frac{\Sigma_{k\in G}\pi_k}{|G|}$, where $G\triangleq\bigcup_{j=1}^{n}G_{(\theta,\phi)_j}$ by aggregating grid point sets $G_{(\theta,\phi)_j}$ generated from all known threat directions (θ,ϕ). We also provide two examples of the non-overlap and overlap instances for the AGP approach in Figures 3.11 and 3.12, respectively.

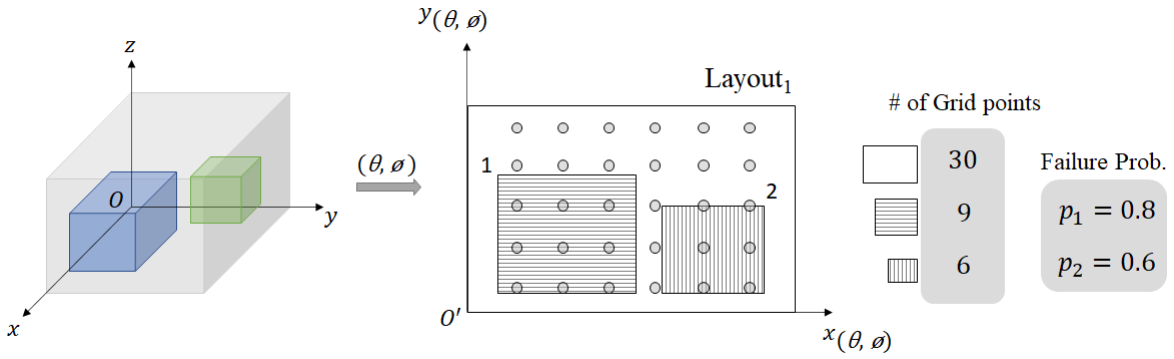

Figure 3.11: Example of the approximated grid point approach with non-overlap areas.

In Figure 3.11, two components 1 and 2 are placed in the exterior hull without any overlaps. The number of grid points in each projected area and the corresponding failure probabilities are also provided. Using Eq. (3.5), the vulnerability from the known threat direction (θ, ϕ) can be calculated as the following:

$$v(\theta,\phi) = \frac{\Sigma_{k \in G_{(\theta,\phi)}} \pi_k}{G_{(\theta,\phi)}} = \frac{9(0.8)+6(0.6)}{30} = 0.36.$$

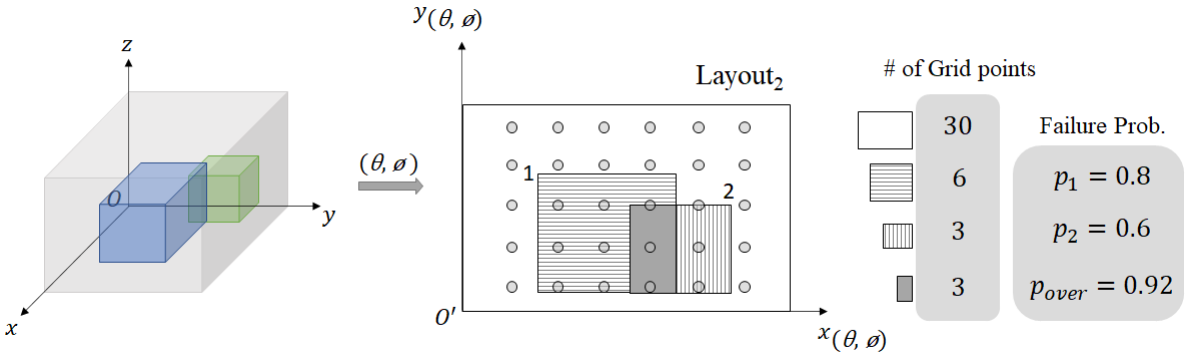

Figure 3.12: Example of the approximated grid point approach with overlap areas.

Additional example including an overlap area is presented in Figure 3.12, with one overlap area and two non-overlap areas. The failure probability of the overlap area (p_{ovrlp}) can be computed by the same manner as Figure 3.8. Then the vulnerability can be calculated

as the following:

$$v(\theta,\phi)=\frac{\Sigma_{k\in G_{(\theta,\phi)}}\pi_k}{G_{(\theta,\phi)}}=\frac{6(0.8)+3(0.6)+3(0.92)}{30}=0.312.$$

We have presented some examples for both of the VA approach and the AGP approach. It is not necessarily the result from the two approaches are the same. Nevertheless, the AGP approach has multiple advantages. First, we can easily capture vulnerability into a mathematical model since complicated shapes of areas no longer need to be calculated individually. We explain in detail how the AGP approach is formulated in Section 4.4. Besides, compared to [Jee18], the grid point approach enables us to obtain closer shapes to the original ones. Also, it is easy to see that the results of the AGP approach converge arbitrarily close to the one from the VA approach as the density of the grid increases.

CHAPTER

4

OPTIMAL COMPONENT LAYOUT PROBLEM

In this chapter, a mathematical model is formulated by using the approximated grid point (AGP) approach discussed in Section 3.3. We first provide a problem statement of the optimal component layout for the minimal weapon vulnerability in Section 4.1. Notations are introduced in Section 4.2. Then we formulate constraints for feasible component layouts in the 3-dimensional (3D) space in Section 4.3, and constraints of adopting the AGP approach in Section 4.4. For practical applications, we add some constraints of adopting the concepts of partial penetration and component redundancy in Sections 4.5 and 4.6, respectively. In Section 4.7, we formulate an objective function to minimize the weapon vulnerability and linearize it using the concept of pseudo-Boolean expressions.

4.1 Problem Statement

The optimal component layout problem determines the 3D coordinates of the given components inside the exterior hull of a weapon system to minimize its vulnerability. Required

information includes the 3D size: length (l_i), width (w_i), and height (h_i), probability of failure (p_i), and resistance to threat (r_i) of each component, as shown in Figure 4.1. Also, enemy's threat directions (θ, ϕ) and initial penetration capacity (β_0) of the enemy's threat are given.

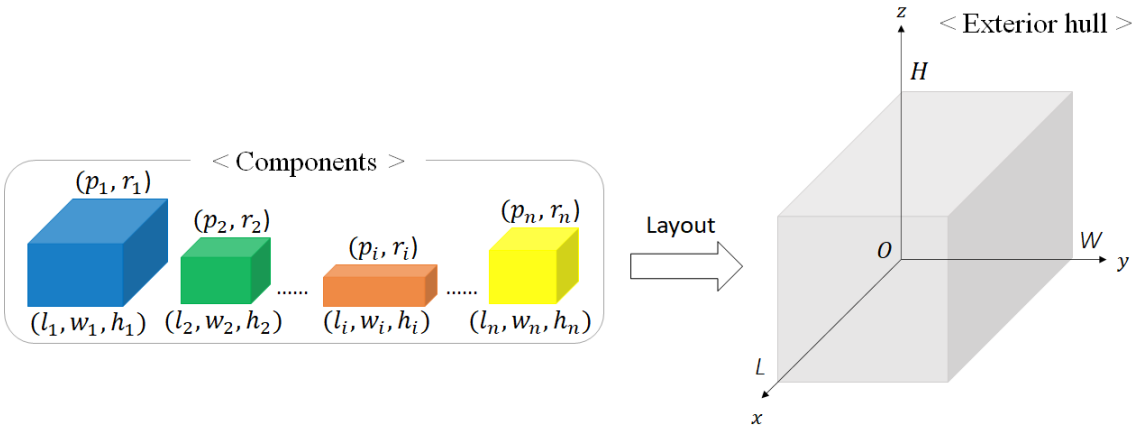

Figure 4.1: Optimal component layout problem.

Additionally, the optimal component layout problem is formulated under the assumptions as below.

- All the components and exterior hull are cuboid-shapes.
- The exterior hull has enough space that can contain all the given components.
- The enemy's threat is a non-explosive penetrating warhead with a single hit.
- The number of threat directions is finite.
- The enemy's threat has a limited penetration capability.

4.2 Notations

Some notations to be used in the mathematical model are given below.

Sets

S : The set of N components to be located,

S_c : The set of N_c critical components,

S_R : The set of N_R redundant components,

S_N : The set of N_N non-critical components,

G : The set of N_G grid points.

Parameters

for $i \in S$ and $k \in G$,

$p_i \in [0,1)$: Probability of failure of the i^{th} component when hit,

$(l_i, w_i, h_i) \in \mathbf{R}^3_{++}$: Length, width, and height of the i^{th} component,

$(L, W, H) \in \mathbf{R}^3_{++}$: Length, width, and height of the exterior hull of a weapon system,

$\mathbf{a}^i_m \in \mathbf{R}^2$: Normal vector of the m^{th} inequality enclosing the i^{th} component's projected area,

$\mathbf{x}^k \in \mathbf{R}^2$: 2D coordinates of the k^{th} grid point,

$r_i \in \mathbf{R}_{++}$: Resistance of the i^{th} component to an enemy's threat (m/s),

$\beta_0 \in \mathbf{R}_{++}$: Initial penetration capability of the enemy's threat (warhead), (m/s).

Decision variables

for $i, j \in S$ and $k \in G$,

$(x_i, y_i, z_i) \in \mathbf{R}^3_{++}$: 3D Coordinates of the centroid of i^{th} component,

$$s_i^k = \begin{cases} 1, & \text{if the projected area of the } i^{\text{th}} \text{ component includes the } k^{\text{th}} \text{ grid point,} \\ 0, & \text{otherwise,} \end{cases}$$

$$t_i^k = \begin{cases} 1, & \text{if the } i^{th} \text{ component is hit at the } k^{\text{th}} \text{ grid point,} \\ 0, & \text{otherwise,} \end{cases}$$

$$\delta_{i,j}^k = \begin{cases} 1, & \text{if the } i^{\text{th}} \text{ component gets hit earlier than the } j^{\text{th}} \text{ one at the } k^{\text{th}} \text{ grid} \\ & \text{point on the given threat direction } (i < j), \\ 0, & \text{otherwise.} \end{cases}$$

4.3 Feasible Component Layout in the 3D Space

We introduce some constraints for a feasible component layout inside a given 3D exterior hull. There exist some related works for the feasible layout of cuboids [Bar02; Her91; Jee18; Sch13]. The basic idea is that each pair of components cannot be overlapped in the 3D space. Thus, at least one of the following three constraints in Eq.(4.1) holds:

$$\begin{aligned} |\, x_i - x_j \,| &\geq (l_i + l_j)/2, \qquad \forall i < j \in S, \\ \text{or} \quad |\, y_i - y_j \,| &\geq (w_i + w_j)/2, \qquad \forall i < j \in S, \\ \text{or} \quad |\, z_i - z_j \,| &\geq (h_i + h_j)/2, \qquad \forall i < j \in S. \end{aligned} \tag{4.1}$$

There are some ways to obtain a set of equivalent linear equations for Eq. (4.1) [Bar02; Her91; Jee18]. We consider the constraints in [Jee18] by adopting additional six binary variables ($b_n^{i,j} \in \{0,1\}, n = 1,2,\ldots,6$) for every component pair (i,j).

$$x_i - x_j \geq (l_i + l_j)/2 + M(b_1^{i,j} - 1), \qquad \forall i < j \in S, \tag{4.2a}$$

$$-x_i + x_j \geq (l_i + l_j)/2 + M(b_2^{i,j} - 1), \qquad \forall i < j \in S, \tag{4.2b}$$

$$y_i - y_j \geq (w_i + w_j)/2 + M(b_3^{i,j} - 1), \qquad \forall i < j \in S, \tag{4.2c}$$

$$-y_i + y_j \geq (w_i + w_j)/2 + M(b_4^{i,j} - 1), \qquad \forall i < j \in S, \tag{4.2d}$$

$$z_i - z_j \geq (h_i + h_j)/2 + M(b_5^{i,j} - 1), \qquad \forall i < j \in S, \tag{4.2e}$$

$$-z_i + z_j \geq (h_i + h_j)/2 + M(b_6^{i,j} - 1), \qquad \forall i < j \in S, \tag{4.2f}$$

$$\sum_{n=1}^{6} b_n^{i,j} \geq 1, \qquad \forall i < j \in S, \tag{4.2g}$$

$$b_n^{i,j} \in \{0,1\}, \qquad n = 1,2,\ldots,6, \forall i < j \in S, \tag{4.2h}$$

where $M = \max_{i,j \in S, i<j} \{\frac{l_i + l_j}{2} + L; \frac{w_i + w_j}{2} + W; \frac{h_i + h_j}{2} + H\}$.

Additionally, every component should be located inside the exterior hull. It is assumed that one of the left bottom vertices of the exterior hull is located at the origin of the 3D space to place the exterior hull in $\mathbf{R}^3_{++}$. Since every component has different sizes $(l_i, w_i, h_i), \forall i \in S$ in the 3D space, the centroid of each component has the lower and upper bounds as the

followings:

$$x_i \in [l_i/2, L - l_i/2], \qquad \forall i \in S, \tag{4.3a}$$

$$y_i \in [w_i/2, W - w_i/2], \qquad \forall i \in S, \tag{4.3b}$$

$$z_i \in [h_i/2, H - h_i/2], \qquad \forall i \in S. \tag{4.3c}$$

4.4 Constraints for the Approximated Grid Point Approach

For adopting the proposed AGP approach discussed in Section 3.3, we need to distinguish whether every grid point is included in each component's projected area. A projected cuboid onto the 2D space may be a four or six-sided figure, as shown in Subsection 3.1.3. Given a projected quadrilateral or hexagon, we can represent the projected area using four or six inequalities. Figure 4.2 illustrates the projected area of a component i surrounded by four linear inequalities, say, $(\mathbf{a}^i_m)^T\mathbf{x} \geq e^i_m, \forall i \in S, m = 1,2,3,4$, where $\mathbf{a}^i_m$ is the normal vector and e^i_m is the intercept.

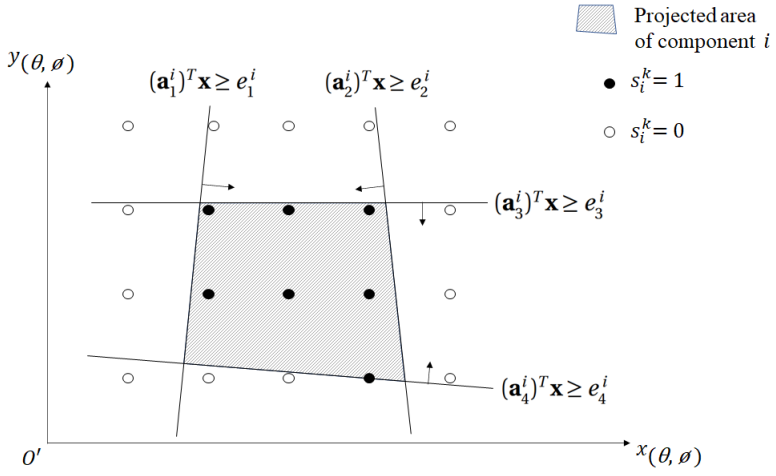

Figure 4.2: Projected area of component i and grid points.

As discussed in Subsection 3.1.3, the normal vector $\mathbf{a}^i_m$ $(\forall i \in S, m = 1,2,...,4(6))$ depends on the size of cuboids $(l_i, w_i, h_i), \forall i \in S$, and threat directions (θ, ϕ). Thus, the normal vectors $\mathbf{a}^i_m$ $(\forall i \in S, m = 1,2,...,4(6))$ are independent of the centroid of components $(x_i, y_i, z_i), \forall i \in S$. The intercept e^i_m can be represented by the linear combination of the

centroid of the cuboid $(x_i, y_i, z_i), \forall i \in S$. Consequently, the linear inequalities, $(\mathbf{a}_m^i)^T \mathbf{x}^k \geq e_m^i, \forall i \in S, m = 1,2,3,4(6)$, are represented by the linear combination of the centroid of cuboids $(x_i, y_i, z_i), \forall i \in S$, where $\mathbf{x}^k$ is the 2D coordinate of grid point k.

Define that $s_i^k = 1$ if grid point k is located inside the projected area of component i, otherwise $s_i^k = 0$. If $\mathbf{x}^k$ satisfies the inequalities $(\mathbf{a}_m^i)^T \mathbf{x}^k \geq e_m^i$ $(\forall i \in S, m = 1,2,\ldots,4(6))$, then the binary variable s_i^k has to be one. This logic can be achieved by the following MILP system:

$$\max \sum_{k \in G} \sum_{i \in S} M_2 s_i^k \tag{4.4a}$$

$$\text{s.t. } (\mathbf{a}_m^i)^T \mathbf{x}^k \geq e_m^i + M_3(s_i^k - 1), \qquad m = 1,2,...,4 \text{ (or } 6), \forall i \in S, k \in G, \tag{4.4b}$$

$$s_i^k \in \{0,1\}, \qquad \forall i \in S, k \in G, \tag{4.4c}$$

where $M_2 = |G|$ and $M_3 = \max_{i,k,m}\{e_m^i - (\mathbf{a}_m^i)^T \mathbf{x}^k\}$.

4.5 Partial Penetration

The vulnerable area approach does not consider partial penetration since it computes vulnerability based on only the vulnerable areas as discussed in Section 3.2. However, for practical applications, it is necessary to assume that the enemy's threat may have a limited penetration capability. When components are overlapped at the same grid point, some components may be intact, which means the warhead as the enemy's threat may not reach some components behind other components. It depends on the warhead's penetration capability (β_0), the resistances (r_i) of the overlap components, and the arrangement sequence $(\delta_{i,j}^k)$ of components at grid point k.

Define that $\delta_{i,j}^k = 1$ if component i gets hit before component j at grid point k from a known threat direction, otherwise $\delta_{i,j}^k = 0$. At grid point k, every layout of a component pair (i, j) can be indicated by using $\delta_{i,j}^k$, s_i^k, and s_j^k $(i < j \in S)$, as shown in Figure 4.3.

For the cases (a), (b), and (c) in Figure 4.3, we can assign proper 0-1 values of the variable $\delta_{i,j}^k$ using the combination of the variables s_i^k and s_j^k. However, when both components i and j are overlapped at the same grid point k, (s_i^k, s_j^k)=(1,1), as shown in the cases (d) and (e) in Figure 4.3, we need to determine the sequence of the components i and j. This arrangement sequence $(\delta_{i,j}^k)$ can be determined by comparing intercepts of the two hyperplanes that include the centroids of the two components i and j. The concept of

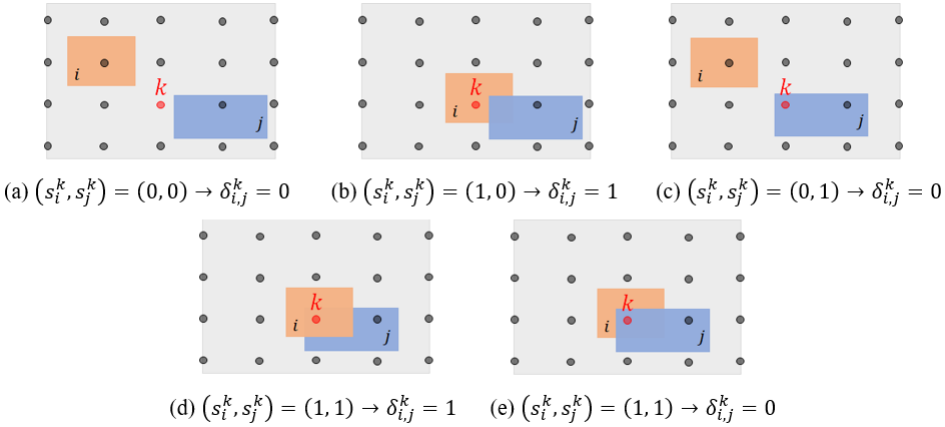

Figure 4.3: Every possible layout of a component pair (i, j) at grid point k.

sequence of overlapped components was investigated in [Jee19]. Notice that a known threat direction (θ, ϕ) can be represented by a 3D vector $\mathbf{a} \triangleq (-\cos\theta, -\sin\theta, -\tan\phi)$. Figure 4.4 illustrates two hyperplanes including the two cuboids' centroid (x_i, y_i, z_i) and (x_j, y_j, z_j) with the normal vector $\mathbf{a}$. Then, we can determine which component is behind the other one by comparing the intercepts d_i and d_j. In Figure 4.4, the component j is behind the component i since $d_i < d_j$. Thus, we can identify the sequence of an overlap component pair (i, j) by using the new variable $d_i (i \in S)$, which is represented by a linear combination of the centroid of component $i (\in S)$.

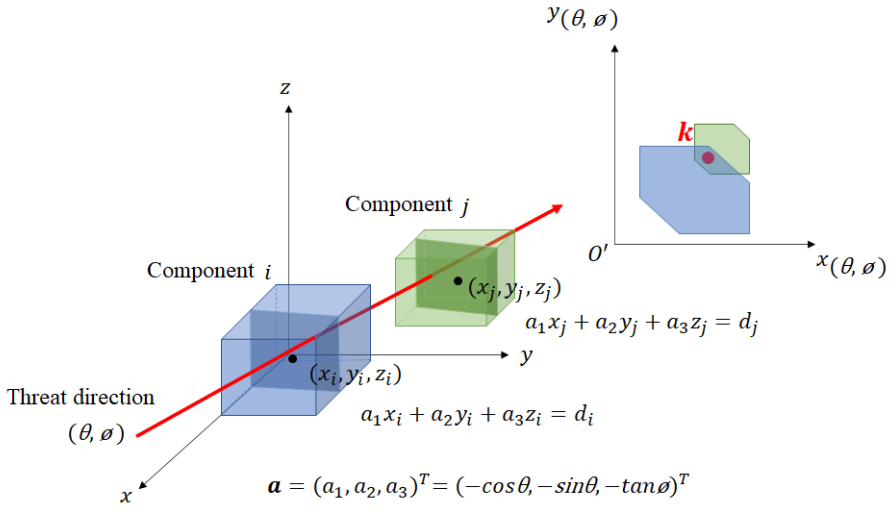

Figure 4.4: Overlap sequence of a component pair (i, j) at grid point k.

Eqs. (4.5a)-(4.5e) explain how the binary variables $\delta^k_{i,j}$ can be determined by s^k_i, s^k_j, d^k_i, and d^k_j in detail. When both components i and j do not include grid point k, (s^k_i, s^k_j)=(0,0), then $\delta^k_{i,j}$ is forced to be zero by Eq. (4.5a). If (s^k_i, s^k_j)=(1,0) or (0,1), then $\delta^k_{i,j} = 1$ or 0 by Eqs. (4.5b) and (4.5c), respectively. Unless (s^k_i, s^k_j)=(1,1), Eqs. (4.5d) and (4.5e) does not provide any restrictions and the binary variable $\delta^k_{i,j}$ is determined by Eqs. (4.5a)-(4.5c). Only when both components i and j are overlapped at the same grid point k, i.e., (s^k_i, s^k_j)=(1,1), we then compare d_i and d_j to determine whether $\delta^k_{i,j} = 1$ or 0 by Eqs. (4.5d) and (4.5e). When $\delta^k_{i,j} = 1$ with (s^k_i, s^k_j)=(1,1), then $d_i < d_j$ by Eq. (4.5d), which means component j is located behind component i. On the contrary, if $\delta^k_{i,j} = 0$ with (s^k_i, s^k_j)=(1,1), then $d_i > d_j$ by Eq. (4.5e), which implies component i is behind component j.

$$s^k_i + s^k_j \geq \delta^k_{i,j}, \qquad \forall i < j \in S, k \in G, \tag{4.5a}$$

$$s^k_i - s^k_j \leq \delta^k_{i,j}, \qquad \forall i < j \in S, k \in G, \tag{4.5b}$$

$$1 + s^k_i - s^k_i \geq \delta^k_{i,j}, \qquad \forall i < j \in S, k \in G, \tag{4.5c}$$

$$M_4(s^k_i + s^k_j - 2) + d_i < d_j + M_4(1 - \delta^k_{i,j}), \qquad \forall i < j \in S, k \in G, \tag{4.5d}$$

$$M_4(s^k_i + s^k_j - 2) + d_j < d_i + M_4\delta^k_{i,j}, \qquad \forall i < j \in S, k \in G, \tag{4.5e}$$

$$\delta^k_{i,j} \in \{0,1\}, \qquad \forall i < j \in S, k \in G, \tag{4.5f}$$

where $M_4 = \max_{i,j \in S, i<j}\{d_j - d_i\}$.

Figure 4.5 shows an instance of a layout with 5 components, $S = \{1,2,3,4,5\}$. Components 2, 3, and 4 are overlapped at the grid point k, $(s^k_1, s^k_2, s^k_3, s^k_4, s^k_5)$=(0,1,1,1,0). By Eqs. (4.5a) and (4.5c), $(\delta^k_{1,2}, \delta^k_{1,3}, \delta^k_{1,4}, \delta^k_{1,5})$ should be (0,0,0,0). The variables $(\delta^k_{2,5}, \delta^k_{3,5}, \delta^k_{4,5})$ are forced to be (1,1,1) by Eq. (4.5b), and $(\delta^k_{2,3}, \delta^k_{2,4}, \delta^k_{3,4})$=(1,0,0) by comparing d^k_i and d^k_j ($d_4 < d_2 < d_3$) using Eqs. (4.5d) and (4.5e), respectively.

The warhead penetration capacity β_0 can be explained as the initial velocity of the warhead (m/s). The resistance of component i (r_i) is determined by its material density and thickness, which can be defined as the decreased velocity of the warhead after penetrating the component i. The approximated linearity for β_0 and r_i was investigated in [Jee19].

Define that $t^k_i = 1$ if component i is hit at grid point k, otherwise $t^k_i = 0$. To clarify if a component is hit at grid point k, it is necessary to obtain an equation representing the residual penetration capacity when a warhead reaches at component i. For example, in Figure 4.5, component 3 may be intact although $s^k_3 = 1$. It depends on the warhead's initial penetration capability (β_0), the resistances of components 2, 3, and 4 (r_2, r_3, r_4), and

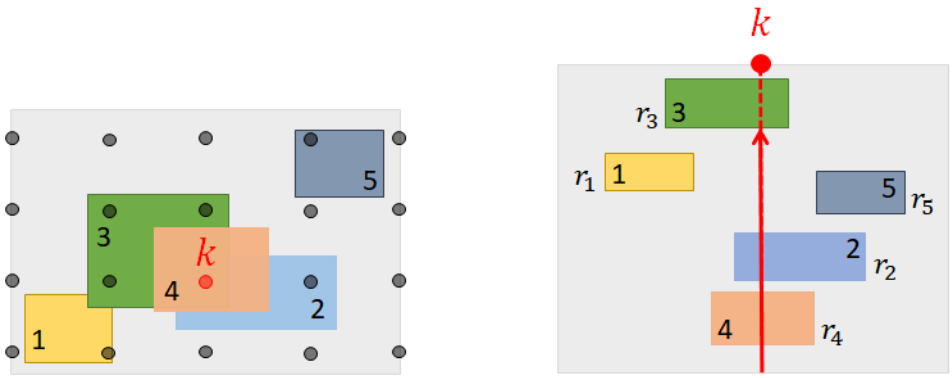

< View from a known threat direction > < View from the top of the threat direction >

Figure 4.5: Instance of 5 component layout.

the component sequence at grid point k ($\delta^k_{i,j}$). In Figure 4.5, when a warhead reaches component 3, the residual penetration capacity at grid point k can be represented by $\beta^k_3 \triangleq \beta_0 - \{r_1\delta^k_{1,3} + r_2\delta^k_{2,3} + r_4(1-\delta^k_{3,4}) + r_5(1-\delta^k_{3,5})\} = \beta_0 - (r_2+r_4)$ since $(\delta^k_{1,3}, \delta^k_{2,3}, \delta^k_{3,4}, \delta^k_{3,5}) = (0,1,0,1)$. Then, we may compare the residual capacity β^k_3 with the resistance of component 3 (r_3) to determine whether t^k_3 should be one or zero.

Only when $s^k_i = 1$, the variable t^k_i needs to be considered. Thus, unless grid point k is located inside the projected area of component i, $s^k_i = 0$ implies $t^k_i = 0$ by Eq. (4.6a). When grid point k is in the projected area of components i, $s^k_i = 1$, then either of Eqs. (4.6b) or (4.6c) holds. In Eqs. (4.6b) and (4.6c), the term $\beta^k_i \triangleq \beta_0 - \{\sum_{j<i} r_j\delta^k_{j,i} + \sum_{j>i} r_j(1-\delta^k_{i,j})\}$ represents the residual penetration capacity when a warhead reaches component i at grid point k. That is, if the residual penetration capacity is greater than or equal to the resistance of component i, i.e., $\beta^k_i \geq r_i$, then component i needs to get hit, i.e., $t^k_i = 1$ by Eq. (4.6b). Otherwise, the variable t^k_i is forced to be zero by Eq. (4.6c).

$$s^k_i \geq t^k_i, \qquad \forall i \in S, k \in G. \tag{4.6a}$$

$$-\beta_0(1-t^k_i) + r_i \leq \beta^k_i + \beta_0(1-s^k_i), \qquad \forall i \in S, k \in G, \tag{4.6b}$$

$$\beta_0(1-s^k_i) + r_i > \beta^k_i - \beta_0 t^k_i, \qquad \forall i \in S, k \in G, \tag{4.6c}$$

$$t^k_i \in \{0,1\}, \qquad \forall i \in S, k \in G, \tag{4.6d}$$

where $\beta^k_i \triangleq \beta_0 - \{\sum_{j<i} r_j\delta^k_{j,i} + \sum_{j>i} r_j(1-\delta^k_{i,j})\}, \forall i \in S, k \in G$.

4.6 Redundant Components

Some critical components may have a spare component that plays as a backup when the corresponding critical component becomes disabled. The spare components are called redundant components. A pair of critical and its corresponding redundant component is connected to the same combat function. Thus, only when both components get disabled, the failure of the combat function really occurs. Redundant components are dealt with in the mathematical model for pragmatic applications.

The set of redundant components is denoted as S_R ($S_R \subsetneq S$ and $S_R \cap S_c = \emptyset$). For component i belonging to S_R, there exists a corresponding critical component $i' \in S_c$ and we create a corresponding $\bar{i}$ which is not in S. The index $\bar{i}$ is not an actual component, but it is necessary to clarify the relation of both of components i ($\in S_R$) and i' ($\in S_c$). Additionally, we define $\overline{S_c} \triangleq S_c \cup \{\bar{i} | i \in S_R \text{ and } i' \in S_c\} \backslash \{i' | i \in S_R \text{ and } i' \in S_c\}$ by replacing those i's in S_c with $\bar{i}$s. For instance, the component set $S = \{1,2,3',4',3,4,5,6\}$ including two (i,i') pairs originally has the subsets $S_c = \{1,2,3',4'\}$, $S_R = \{3,4\}$, and $S_N = \{5,6\}$. Then the set $\overline{S_c}$ is defined as $S_c \cup \{\bar{i} | (i,i') \in (S_R, S_c)\} \backslash \{i' | (i,i') \in (S_R, S_c)\} = \{1,2,\bar{3},\bar{4}\}$ with the new indices $\bar{3}$ and $\bar{4}$ representing the component pairs $(3,3')$ and $(4,4')$, respectively.

To indicate if both of the critical and its corresponding redundant components are hit at the same grid point k, we introduce a new binary variable $t_{\bar{i}}^k$ defined as:

$$t_{\bar{i}}^k = \begin{cases} 1, & \text{if both critical component } i' (\in S_c) \text{ and its corresponding redundant} \\ & \text{component } i (\in S_R) \text{ are hit at the } k^{\text{th}} \text{ grid point,} \\ 0, & \text{otherwise.} \end{cases}$$

Figure 4.6 illustrates two possible layouts of critical component i' and its corresponding redundant component i. On the left layout, the critical component i' is hit at a grid point k, but its corresponding redundant component i is intact. The binary variable $t_{\bar{i}}^k$ has to be zero since only one component of the component pair (i,i') is hit. On the right component layout, both of components i and i' are hit at the same grid point k, i.e., $t_i^k = t_{i'}^k = 1$, so the binary variable $t_{\bar{i}}^k$ is forced to be one. If both of components $i (\in S_R)$ and $i' (\in S_c)$ are hit at the same grid point k, i.e., $t_i^k = t_{i'}^k = 1$, then we have $t_{\bar{i}}^k = 1$, which means the function related to component pair (i,i') can be disabled due to the hit. Since either failure of components i or i' does not affect the function disability, the failure probabilities of the triplet components $(i', i, \bar{i})$ are assigned to be $(0, 0, p_{\bar{i}})$, where $p_{\bar{i}} \triangleq p_i \cdot p_{i'}$.

For every redundant component i ($\in S_R$), we can identify component i' ($\in S_c$). Thus, if

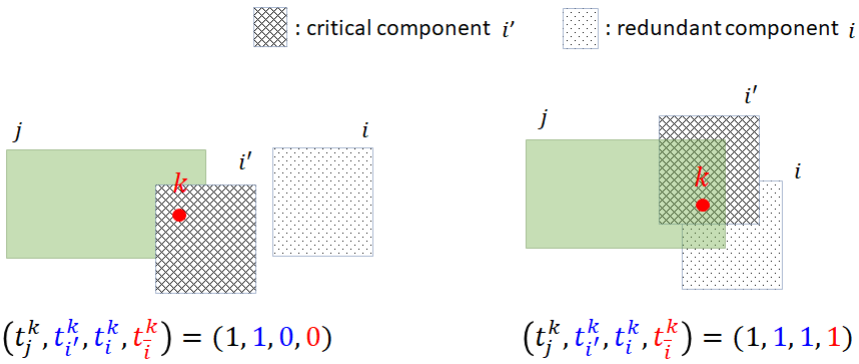

Figure 4.6: Redundant components.

both of components i and i' are hit at grid point k, i.e., $t_i^k = t_{i'}^k = 1$, then the binary variable $t_{\bar{i}}^k$ has to be one by Eq. (4.7a), which implies that the corresponding failure of components i and i' may occur only when both of them are hit.

$$(t_i^k + t_{i'}^k) - 1 \le t_{\bar{i}}^k, \qquad \forall (i, i') \in (S_R, S_c), k \in G, \tag{4.7a}$$

$$t_{\bar{i}}^k \in \{0, 1\}, \qquad \forall \bar{i} \in \overline{S_c}, k \in G. \tag{4.7b}$$

4.7 Objective Function and its Linearization

The objective of the proposed model is to minimize the weapon vulnerability or to maximize the weapon survivability subjected to a hit. As we discussed in Subsection 2.1.1, both concepts of susceptibility (P_H) and vulnerability ($P_{K/H}$) are required to measure weapon survivability (P_S). Since we assume weapon systems are hit, the probability of the weapon survivability given a hit ($P_{S/H}$) can be defined as the followings:

$$\text{Survivability}\,(P_S) = 1 - \text{Susceptibility}\,(P_H) \times \text{Vulnerability}\,(P_{K/H}),$$
$$\text{Survivability given hit}\,(P_{S/H}) = 1 - \text{Vulnerability}\,(P_{K/H}).$$

Given a hit with a known threat direction (θ, ϕ), some components may be overlapped at grid point k. To calculate the failure probability of a weapon system at grid point k, we only consider the disabilities of components in $\overline{S_c}$, which includes the critical components without redundancy and the indices $\bar{i}$s for the pairs of a critical and its corresponding redundant components. Non-critical components are not involved in calculating the failure

probability of a weapon system at grid point k. Based on the components' location with their layout sequence at grid point k ($\delta^k_{i,j}$), the resistance (r_i), and the initial penetration capability (β_0), it is determined if each component in $\overline{S_c}$ is hit or not at grid point k, i.e., $t^k_i = 1$ or 0 ($i \in \overline{S_c}$), respectively. Then the failure probability of a weapon system at grid point k can be defined as $\pi_k \triangleq 1 - \prod_{i \in \overline{S_c}} (1-p_i)^{t^k_i}$ given a hit at the grid point k.

Since a single hit is considered, we assume that the single hit occurs uniformly distributed at each grid point. Then the weapon vulnerability ($P_{K/H}$) can be measured as the average value of the failure probabilities of a weapon (π_k) at all grid points. Thus, the weapon vulnerability $P_{K/H}$ can be represented by $\frac{\sum_{k \in G} \pi_k}{|G|}$ using the grid point set G and the summation of all failure probabilities (π_k) of the weapon system at all grid points. Consequently, the weapon survivability given a hit $P_{S/H}$ is represented by:

$$\begin{aligned} P_{S/H} &= 1 - P_{K/H} = 1 - \frac{\sum_{k \in G} \pi_k}{|G|} = 1 - \frac{\sum_{k \in G} \{1 - \prod_{i \in \overline{S_c}} (1-p_i)^{t^k_i}\}}{|G|} \\ &= 1 - \frac{|G| - \sum_{k \in G} \prod_{i \in \overline{S_c}} (1-p_i)^{t^k_i}}{|G|} = \frac{\sum_{k \in G} \prod_{i \in \overline{S_c}} (1-p_i)^{t^k_i}}{|G|}. \end{aligned}$$

The number of grid points $|G|$ is given, so the following objective is to be maximized with binary variable t^k_i ($\forall i \in \overline{S_c}, k \in G$):

$$\sum_{k \in G} \prod_{i \in \overline{S_c}} (1-p_i)^{t^k_i}. \tag{4.8}$$

As discussed in Section 4.4, we need to add Expression (4.4a), $\sum_{k \in G} \sum_{i \in S} M_2 s^k_i$, to the objective function for adopting the AGP approach. Combining Expressions (4.4a) and (4.8), the objective function of the proposed model to be maximized becomes $\sum_{k \in G} \sum_{i \in S} M_2 s^k_i + + \sum_{k \in G} \prod_{i \in \overline{S_c}} (1-p_i)^{t^k_i}$. The constraints for feasible component layout in the 3D space, AGP approach, partial penetration, and redundant components, i.e., Eqs. (4.2a)-(4.3c), (4.4b)-(4.4c), (4.5a)-(4.6d), and (4.7a)-(4.7b), are also included in the proposed model, respectively. This leads the following mathematical model:

$$\max \sum_{k \in G} \sum_{i \in S} M_2 s^k_i + \sum_{k \in G} \sum_{i \in \overline{S_c}} (1-p_i)^{t^k_i} \qquad \text{(4.4a and 4.8)}$$

$$\text{s.t. } x_i - x_j \geq (l_i + l_j)/2 + M(b_1^{i,j} - 1), \qquad \forall i < j \in S, \qquad \text{(4.2a)}$$

$$-x_i + x_j \geq (l_i + l_j)/2 + M(b_2^{i,j} - 1), \qquad \forall i < j \in S, \qquad \text{(4.2b)}$$

$$y_i - y_j \geq (w_i+w_j)/2 + M(b_3^{i,j}-1), \qquad \forall i<j\in S, \tag{4.2c}$$

$$-y_i + y_j \geq (w_i+w_j)/2 + M(b_4^{i,j}-1), \qquad \forall i<j\in S, \tag{4.2d}$$

$$z_i - z_j \geq (h_i+h_j)/2 + M(b_5^{i,j}-1), \qquad \forall i<j\in S, \tag{4.2e}$$

$$-z_i + z_j \geq (h_i+h_j)/2 + M(b_6^{i,j}-1), \qquad \forall i<j\in S, \tag{4.2f}$$

$$\sum_{n=1}^{6} b_n^{i,j} \geq 1, \qquad \forall i<j\in S, \tag{4.2g}$$

$$(\mathbf{a}_m^i)^T \mathbf{x}^k \geq e_m^i + M_3(s_i^k-1), \qquad m=1,2,...,4\,(\text{or } 6), \forall i\in S, k\in G, \tag{4.4b}$$

$$s_i^k + s_j^k \geq \delta_{i,j}^k, \qquad \forall i<j\in S, k\in G, \tag{4.5a}$$

$$s_i^k - s_j^k \leq \delta_{i,j}^k, \qquad \forall i<j\in S, k\in G, \tag{4.5b}$$

$$1 + s_i^k - s_i^k \geq \delta_{i,j}^k, \qquad \forall i<j\in S, k\in G, \tag{4.5c}$$

$$M_4(s_i^k + s_j^k - 2) + d_i < d_j + M_4(1-\delta_{i,j}^k), \qquad \forall i<j\in S, k\in G, \tag{4.5d}$$

$$M_4(s_i^k + s_j^k - 2) + d_j < d_i + M_4\delta_{i,j}^k, \qquad \forall i<j\in S, k\in G, \tag{4.5e}$$

$$s_i^k \geq t_i^k, \qquad \forall i\in S, k\in G, \tag{4.6a}$$

$$-\beta_0(1-t_i^k) + r_i \leq \beta_i^k + \beta_0(1-s_i^k), \qquad \forall i\in S, k\in G, \tag{4.6b}$$

$$\beta_0(1-s_i^k) + r_i > \beta_i^k - \beta_0 t_i^k, \qquad \forall i\in S, k\in G, \tag{4.6c}$$

$$(t_i^k + t_{i'}^k) - 1 \leq t_{\tilde{i}}^k, \qquad \forall (i,i')\in (S_R, S_c), k\in G, \tag{4.7a}$$

$$x_i \in [l_i/2, L-l_i/2], \qquad \forall i\in S, \tag{4.3a}$$

$$y_i \in [w_i/2, W-w_i/2], \qquad \forall i\in S, \tag{4.3b}$$

$$z_i \in [h_i/2, H-h_i/2], \qquad \forall i\in S, \tag{4.3c}$$

$$b_n^{i,j} \in \{0,1\}, \qquad n=1,2,...,6, \forall i<j\in S, \tag{4.2h}$$

$$s_i^k \in \{0,1\}, \qquad \forall i\in S, k\in G, \tag{4.4c}$$

$$\delta_{i,j}^k \in \{0,1\}, \qquad \forall i<j\in S, k\in G, \tag{4.5f}$$

$$t_i^k \in \{0,1\}, \qquad \forall i\in S\cup\overline{S_c}, k\in G, \tag{4.6d and 4.7b}$$

where $M = \max_{i,j\in S, i<j}\{\frac{l_i+l_j}{2}+L; \frac{w_i+w_j}{2}+W; \frac{h_i+h_j}{2}+H\}$, $M_2 = |G|$, $M_3 = \max_{i,k,m}\{e_m^i - (\mathbf{a}_m^i)^T\mathbf{x}^k\}$, $M_4 = \max_{i,j\in S, i<j}\{d_j - d_i\}$, and $\beta_i^k \triangleq \beta_0 - \{\sum_{j<i} r_j\delta_{j,i}^k + \sum_{j>i} r_j(1-\delta_{i,j}^k)\}, \forall i\in S, k\in G$.

This model includes some continuous variables $(x_i, y_i, z_i), \forall i\in S$ and both e_m^i ($m = 1,\ldots,4(6), \forall i\in S$) and d_i ($\forall i\in S$) are represented by the linear combination of $(x_i, y_i, z_i), \forall i\in$

S, as mentioned in Sections 4.4 and 4.5, respectively. The binary variables consist of $b_n^{i,j}$ ($n = 1,2,\ldots,6,\ \forall i < j \in S$), s_i^k ($\forall i \in S, k \in G$), $\delta_{i,j}^k$ ($\forall i < j \in S, k \in G$), and t_i^k ($\forall i \in S \cup \overline{S_c}, k \in G$). The parameters (l_i, w_i, h_i), r_i, p_i, ($\forall i \in S$), (L, W, H), β_0, $\mathbf{x}^k$, ($\forall k \in G$), and $\mathbf{a}_m^i (m = 1,\ldots,4(6), \forall i \in S)$ are given. The components sets S, S_c, S_R, $\overline{S_c}$, and the grid point set G are also preprocessed. All the constraints are in the linear forms with integer or mixed-integer variables. Here the real issue is the complicated term $\sum_{k\in G}\prod_{i\in\overline{S_c}}(1-p_i)^{t_i^k}$ in the objective function, which consists of the product of exponential functions that is non-convex with binary variables t_i^k ($\forall i \in \overline{S_c}, k \in G$):

$$\sum_{k\in G}\prod_{i\in\overline{S_c}}(1-p_i)^{t_i^k}. \tag{4.8}$$

To handle Expression (4.8), we first show that Expression (4.8) can be converted into a special case of pseudo-Boolean expression. A pseudo-Boolean expression on $\boldsymbol{\tau} \in \mathbf{B}^n = \{0,1\}^n$ is defined in [Cra93]:

$$f(\boldsymbol{\tau}) = \sum_{(T,R)\in\Gamma}\{a_T\prod_{i\in T}\tau_i\prod_{j\in R}(1-\tau_j)\} \tag{4.11}$$

where $\Gamma \subseteq P \triangleq \{(T,R)|T \cup R = \{1,2,...,n\}, T \cap R = \emptyset\}$ and $a_T \neq 0$ are given for all $T \subseteq \{1,2,...,n\}$. The set P actually represents a set of all possible partitions of an index set $\{1,2,...,n\}$.

Since a grid point k may be used by $|\overline{S_c}|$ components indicated by t_i^k ($i \in \overline{S_c}$), we have $2^{|\overline{S_c}|}$ possible combinations. We consider a set of every possible partition of $\overline{S_c}$, i.e., $P \triangleq \{(T,R)|T \cup R = \overline{S_c}, T \cap R = \emptyset\}$. Let sets T and R be $\{i \in \overline{S_c}|t_i^k = 1\}$ and $\{i \in \overline{S_c}|t_i^k = 0\}$, respectively. Then each partition in P has a one-to-one correspondence to a combination with t_i^k ($i \in \overline{S_c}$,). We consider the summation of the product terms derived from every possible partition as the following:

$$\sum_{(T,R)\in P}\{\prod_{i\in T}(1-p_i)t_i^k\prod_{j\in R}(1-t_j^k)\}. \tag{4.12}$$

For any combination of t_i^k ($i \in \overline{S_c}$), we can identify a corresponding partition (T,R) in P. If t_i^k ($i \in \overline{S_c}$) is specified, only the corresponding term $\prod_{i\in T}(1-p_i)t_i^k\prod_{j\in R}(1-t_j^k)$ in the summation of Expression (4.12) can have a value of $\prod_{i\in T}(1-p_i)$. Other terms become zero. Thus, Expressions (4.8) and (4.12) have a one-to-one correspondence. The failure probability p_i of component $i(\in \overline{S_c})$ are in the range of $(0,1)$ since the component set $\overline{S_c}$ does not include any non-critical components. We can define $\alpha_T \triangleq \prod_{i\in T}(1-p_i)$, then $\alpha_T \in (0,1)$, $\forall T \subseteq P$. In this way, Expression (4.12) can be rewritten as follows:

$$\sum_{(T,R)\in P} \{\alpha_T \prod_{i\in T} t_i^k \prod_{j\in R} (1-t_i^k)\}, \tag{4.13}$$

where $P = \{(T,R) | T \cup R = \overline{S_c}, T \cap R = \emptyset\}$, $\alpha_T \in (0,1)$, $\forall T \subseteq P$. Compared to Eq. (4.11), Expression (4.13) has the entire partition set P instead of a subset Γ. The given parameter $\alpha_T (\in (0,1))$ corresponds to $a_T (\neq 0)$. Thus, Expression (4.13) is a special case of the pseudo-Boolean expression (4.11).

By now, Expression (4.8) has been converted to Expression (4.13), which is a special case of pseudo-Boolean expression. The next Lemma 1 [Cra93; Fal76; Roc70] provides a concave envelope of Expression (4.13).

[Cra93] Let by $\mathbf{x}^1, \mathbf{x}^2, \ldots, \mathbf{x}^N$ be the 2^n elements of $\mathbf{B}^n = \{0,1\}^n$. If f is a pseudo-Boolean expression defined on $\mathbf{B}^n$, then the concave envelope $f^C(\mathbf{x})$ on $\mathbf{x} \in [0,1]^n$ is provided by:

$$\begin{aligned} f^C(\mathbf{x}) = \quad & \max \quad \sum_{m=1}^{N} \lambda_m f(\mathbf{x}^m) \\ & \text{s.t.} \quad \sum_{m=1}^{N} \lambda_m \mathbf{x}^m = \mathbf{x}, \\ & \qquad \sum_{m=1}^{N} \lambda_m = 1, \\ & \qquad \lambda_m \geq 0, \qquad\qquad m = 1,2,...,N. \end{aligned} \tag{4.14}$$

Moreover, the maximum of $f^C(\mathbf{x})$ over $[0,1]^n$ is attained at a 0-1 point, and this maximum is always equal to the maximum of the pseudo-Boolean expression f over $\{0,1\}^n$. ■

Lemma 1 says that the concave envelope of Expression (4.13) is provided by solving:

$$\max \quad \sum_{k\in G} \sum_{T\subseteq \overline{S_c}} \alpha_T \lambda_T^k \tag{4.15a}$$

$$\text{s.t.} \quad \sum_{T\ni i} \lambda_T^k = t_i^k, \qquad \forall i \in \overline{S_c}, k \in G, \tag{4.15b}$$

$$\sum_{T\subseteq \overline{S_c}} \lambda_T^k = 1, \qquad \forall k \in G, \tag{4.15c}$$

$$\lambda_T^k \geq 0, \qquad \forall T \subseteq \overline{S_c}, k \in G, \tag{4.15d}$$

$$t_i^k \in [0,1], \qquad \forall i \in \overline{S_c}, k \in G. \tag{4.15e}$$

The optimum of the linear system of (4.15a)-(4.15e) is achieved at $t_i^k = 0$ or 1, ($\forall i \in \overline{S_c}$, $k \in G$), and this optimum is always equal to the optimum of Expression (4.13) by Lemma 1.

In this way, our objective function can be linearized by introducing the new continuous variables λ_T^k ($\forall T \subseteq \overline{S_c}$, $k \in G$). The relaxed t_i^k in Expression (4.15e) remains to be binary variables because of Eqs. (4.6b) and (4.6c) in the proposed model. Now the mathematical model is reformulated as a mixed-integer linear programming (MILP) model by combining Expressions (4.4a) and (4.15a) in the objective function and Eqs. (4.2a)-(4.3c), (4.4b)-(4.4c), (4.5a)-(4.6d), (4.7a)-(4.7b), and (4.15b)-(4.15d) in the constraints:

$$\max \sum_{k\in G}\sum_{i\in S} M_2 s_i^k + \sum_{k\in G}\sum_{T\subseteq\overline{S_c}} \alpha_T \lambda_T^k \qquad \text{(4.4a and 4.13a)}$$

$$\text{s.t. } x_i - x_j \geq (l_i+l_j)/2 + M(b_1^{i,j}-1), \qquad \forall i<j\in S, \qquad \text{(4.2a)}$$

$$-x_i + x_j \geq (l_i+l_j)/2 + M(b_2^{i,j}-1), \qquad \forall i<j\in S, \qquad \text{(4.2b)}$$

$$y_i - y_j \geq (w_i+w_j)/2 + M(b_3^{i,j}-1), \qquad \forall i<j\in S, \qquad \text{(4.2c)}$$

$$-y_i + y_j \geq (w_i+w_j)/2 + M(b_4^{i,j}-1), \qquad \forall i<j\in S, \qquad \text{(4.2d)}$$

$$z_i - z_j \geq (h_i+h_j)/2 + M(b_5^{i,j}-1), \qquad \forall i<j\in S, \qquad \text{(4.2e)}$$

$$-z_i + z_j \geq (h_i+h_j)/2 + M(b_6^{i,j}-1), \qquad \forall i<j\in S, \qquad \text{(4.2f)}$$

$$\sum_{n=1}^{6} b_n^{i,j} \geq 1, \qquad \forall i<j\in S, \qquad \text{(4.2g)}$$

$$(\mathbf{a}_m^i)^T \mathbf{x}^k \geq e_m^i + M_3(s_i^k - 1), \qquad m=1,2,...,4\,(6), \forall i\in S, k\in G, \qquad \text{(4.4b)}$$

$$s_i^k + s_j^k \geq \delta_{i,j}^k, \qquad \forall i<j\in S, k\in G, \qquad \text{(4.5a)}$$

$$s_i^k - s_j^k \leq \delta_{i,j}^k, \qquad \forall i<j\in S, k\in G, \qquad \text{(4.5b)}$$

$$1 + s_i^k - s_j^k \geq \delta_{i,j}^k, \qquad \forall i<j\in S, k\in G, \qquad \text{(4.5c)}$$

$$M_4(s_i^k + s_j^k - 2) + d_i < d_j + M_4(1-\delta_{i,j}^k), \qquad \forall i<j\in S, k\in G, \qquad \text{(4.5d)}$$

$$M_4(s_i^k + s_j^k - 2) + d_j < d_i + M_4\delta_{i,j}^k, \qquad \forall i<j\in S, k\in G, \qquad \text{(4.5e)}$$

$$s_i^k \geq t_i^k, \qquad \forall i\in S, k\in G, \qquad \text{(4.6a)}$$

$$-\beta_0(1-t_i^k) + r_i \leq \beta_i^k + \beta_0(1-s_i^k), \qquad \forall i\in S, k\in G, \qquad \text{(4.6b)}$$

$$\beta_0(1-s_i^k) + r_i > \beta_i^k - \beta_0 t_i^k, \qquad \forall i\in S, k\in G, \qquad \text{(4.6c)}$$

$$(t_i^k + t_{i'}^k) - 1 \leq t_i^k, \qquad \forall (i,i')\in(S_R,S_c), k\in G, \qquad \text{(4.7a)}$$

$$\sum_{T \ni i} \lambda_T^k = t_i^k, \qquad \forall i \in \overline{S_c}, k \in G, \tag{4.15b}$$

$$\sum_{T \subseteq \overline{S_c}} \lambda_T^k = 1, \qquad \forall k \in G, \tag{4.15c}$$

$$x_i \in [l_i/2, L - l_i/2], \qquad \forall i \in S, \tag{4.3a}$$

$$y_i \in [w_i/2, W - w_i/2], \qquad \forall i \in S, \tag{4.3b}$$

$$z_i \in [h_i/2, H - h_i/2], \qquad \forall i \in S, \tag{4.3c}$$

$$\lambda_T^k \geq 0, \qquad \forall T \subseteq \overline{S_c}, k \in G, \tag{4.15d}$$

$$b_n^{i,j} \in \{0,1\}, \qquad n = 1,2,...,6, \forall i < j \in S, \tag{4.2h}$$

$$s_i^k \in \{0,1\}, \qquad \forall i \in S, k \in G, \tag{4.4c}$$

$$\delta_{i,j}^k \in \{0,1\}, \qquad \forall i < j \in S, k \in G, \tag{4.5f}$$

$$t_i^k \in \{0,1\}, \qquad \forall i \in S \cup \overline{S_c}, k \in G, \tag{4.6d and 4.7b}$$

where $\alpha_T \triangleq \prod_{i \in T}(1-p)$, $M = \max_{i,j \in S, i<j}\{\frac{l_i+l_j}{2} + L; \frac{w_i+w_j}{2} + W; \frac{h_i+h_j}{2} + H\}$, $M_2 = |G|$, $M_3 = \max_{i,k,m}\{e_m^i - (\mathbf{a}_m^i)^T \mathbf{x}^k\}$, $M_4 = \max_{i,j \in S, i<j}\{d_j - d_i\}$, and $\beta_i^k \triangleq \beta_0 - \{\sum_{j<i} r_j \delta_{j,i} + \sum_{j>i} r_j (1 - \delta_{i,j}^k)\}$, $\forall i \in S, k \in G$.

Notice that the proposed MILP model has $3N + 2^{|\overline{S_c}|} \cdot |G|$ continuous variables of $(x_i, y_i, z_i), \forall i \in S$ and $\lambda_T^k (\forall T \subseteq \overline{S_c}, k \in G)$. Also, it includes $3N(N-1) + N \cdot |G| + \frac{1}{2}N(N-1)|G| + (N + |S_R|) \cdot |G|$ binary variables of $b_n^{i,j} (n = 1,2,\ldots,6, \forall i < j \in S)$, $s_i^k (\forall i \in S, k \in G)$, $\delta_{i,j}^k (\forall i < j \in S, k \in G)$, and $t_i^k (\forall i \in S \cup \overline{S_c}, k \in G)$. In terms of constraints, the model has $6N + |G|$ linear constraints in continuous variables, $3N\{3(N-1) + |G| \cdot (|\overline{S_c}| + 6)\}$ linear constraints in mixed-integer variables, and $3N(N-1) + |G| \cdot \{3N(3N-2) + |S_R|\}$ linear constraints in binary variables.

The above MILP model enables us to find optimal component layouts of a weapon system using any commercial software. Some readily available MILP solvers include, but not limed to, ILOG CPLEX [ILO], Gurobi, LINDO, Mosek, XPRESS-MP [Lin11] and AMPL [Ji 19].

CHAPTER

5

HEURISTIC AND NUMERICAL EXPERIMENTS

Although we can solve the proposed mixed-integer linear programming (MILP) model using commercial solvers, we may still suffer from the low computation efficiency caused by a large number of binary variables and constraints. In Section 5.1, we propose a heuristic method to solve the proposed MILP model in a much more efficient manner. In Section 5.2, a practical instance is provided to highlight the proposed MILP model solved by the Branch and Cut (B&C) method and proposed heuristic method. Numerical experiments and analysis are also provided to validate the performance of the proposed heuristic method.

5.1 Zone-based Restriction Heuristic Method

Recall that the weapon vulnerability depends on how components are arranged inside the exterior hull of a weapon system. Using the components' 3D coordinates and known threat directions (θ, ϕ), we can identify what components include a grid point k by the binary variables s_i^k $(\forall i \in S,\ k \in G)$. Then we can distinguish whether each component is hit at the

grid point k or not, i.e., $t_i^k = 1$ or 0 ($\forall i \in S \cup \overline{S_c}, k \in G$) by using the sequences of components pairs ($\delta_{i,j}^k$), the resistance of components (r_i), and the initial penetration capacity of the enemy's threat (β_0). Since the weapon vulnerability is defined as the average value of the failure probabilities at all grid points, $\frac{\sum_{k\in G}\pi_k}{|G|}$, the weapon vulnerability is determined by whether the components in $\overline{S_c}$ is hit or not, with $\pi_k \triangleq 1-\prod_{i\in\overline{S_c}}(1-p_i)^{t_i^k}$.

In this dissertation, we consider four types of components: critical components without redundancy, critical components with redundancy, redundant components, and non-critical components. Notice that a hit on a non-critical component does not directly affect the calculation of weapon vulnerability, but non-critical components can protect other components behind them. Unless a critical component (with redundancy) and its corresponding redundant component are hit at the same grid point, they do not affect the weapon vulnerability either. However, the hit on a critical component (without redundancy) will directly increase the weapon vulnerability. Using these characteristics of component types, the proposed heuristic is designed to properly allocate critical components (with and without redundancy) for better protections. The essence of the proposed heuristic method is to lay out the critical components behind other components. This prevents the critical components from being easily hit by enemy threats. Hence we may want to restrict the feasible region to place the critical components.

We provide an example in the 2-dimensional (2D) space to explain the process of the proposed zone-based restriction heuristic (ZRH) method. Assume that we have a component set $S = \{1, 2, 3', 3, 4\}$ of 5 components including the critical component set $S_c = \{1, 2, 3'\}$, redundant component set $S_R = \{3\}$, and non-critical component set $S_N = \{4\}$. Each component has its own size (l_i, w_i), $\forall i \in S$ and failure probability $p_i(> 0)$, $\forall i \in S \backslash S_N$, with $p_3 = p_{3'} > p_2 > p_1$. We also have a size of an exterior hull (L, W) and threat directions (θ, ϕ).

We first present the feasible region for the components ($\forall i \in S$) using the range of the exterior hull ($[0, L], [0, W]$) and three threat directions: from the top, the left-hand side, and the right-hand side, as shown in Figure 5.1. Then we can identify a point that is the farthest away from the three threat directions in the exterior hull, which is designed as the innermost point I. In Figure 5.1, the innermost point I is located at the point $(L/2, 0)$ in the exterior hull.

We then find the two most vulnerable components in $S_c = \{1, 2, 3'\}$ with higher failure probabilities. Here components 2 and 3′ are chosen since $p_{3'} > p_2 > p_1$, and we have a set $S_1 = \{2, 3'\}$ which denotes the component set to be included in Zone 1. Then we generate Zone 1 to accommodate all possible layouts of the components in $S_1 = \{2, 3'\}$. The generated Zone 1 is then placed close to the innermost point $I(L/2, 0)$, as shown in Figure 5.2.

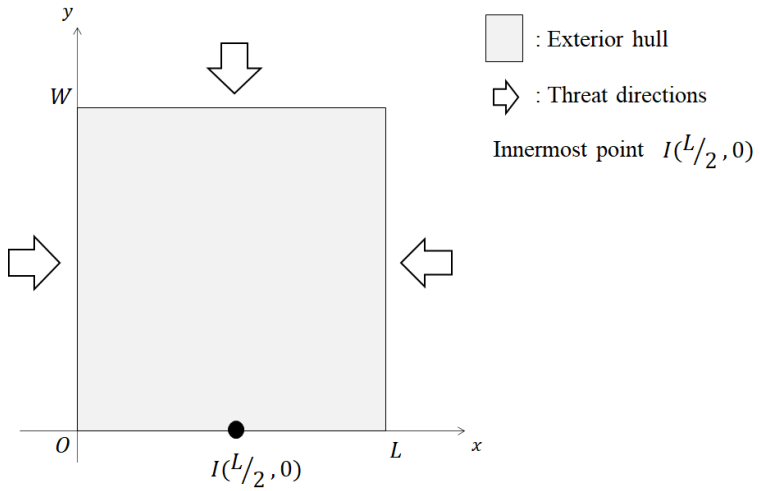

Figure 5.1: Innermost point I.

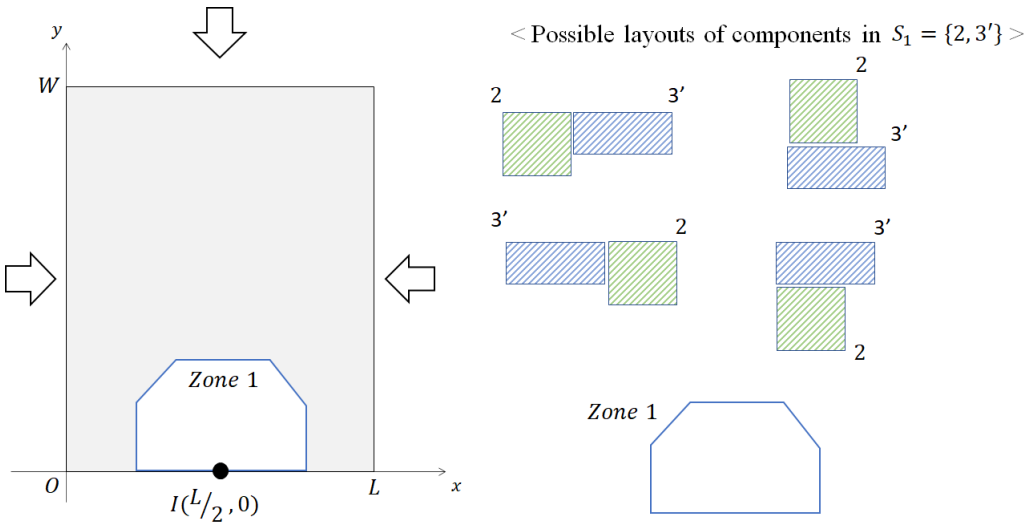

Figure 5.2: Zone 1 accommodating possible layouts of components in S_1.

Then we generate those linear inequalities representing Zone 1 with a given margin $d(> 0)$, as shown in Figure 5.3. The margin helps prevent the critical components from being over-restricted by the linear inequalities. The linear inequalities ①a, ①b, ①c, ①d, and ①e (①a-①e) in Figure 5.3 restricts the critical components in $S_1 = \{2, 3'\}$ to be located

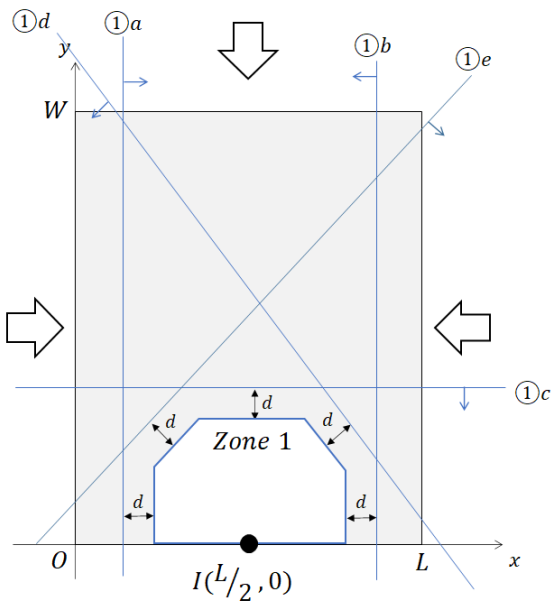

Figure 5.3: Linear inequalities representing Zone 1 with margin $d(>0)$.

inside Zone 1 with the margin d.

Now we check the remaining critical components in S_c, which are not yet assigned to any zones. Currently, only the critical component 1 is left. To generate Zone 2, if we consider the critical component 1 only, it may lead to a too small zone. If we generate Zone 2 to accommodate components 2 and 3′ and the current critical component 1, Zone 2 may become too large. Hence we create a fictitious component v_1 with the size of $(l_{v_1}, w_{v_1}) \triangleq (\max\{l_2, l_{3'}\}, \max\{w_2, w_{3'}\})$, which is called the virtual component v_1 derived from $S_1 = \{2, 3'\}$. Figure 5.4 shows the virtual component v_1 came from $S_1 = \{2, 3'\}$.

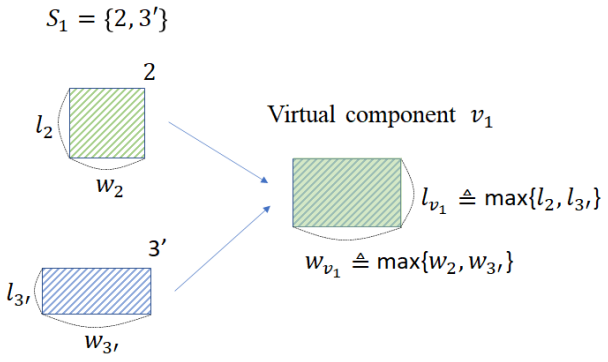

Figure 5.4: Virtual component v_1 derived from S_1.

Now we take the set $S_2 = \{v_1, 1\}$ to include the critical component 1 and the virtual component v_1. Subsequently, Zone 2 is generated to accommodate all possible layouts of components in $S_2 = \{v_1, 1\}$, and place it close to the innermost point $I(L/2, 0)$, as shown in Figure 5.5.

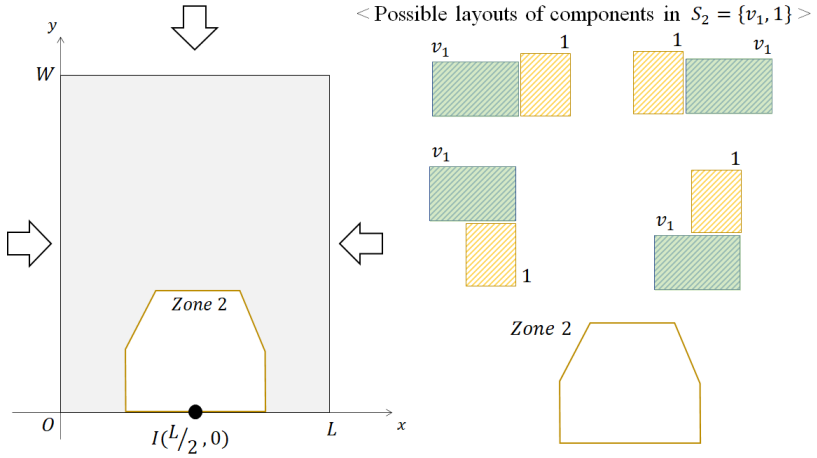

Figure 5.5: Zone 2 accommodating possible layouts of components in S_2.

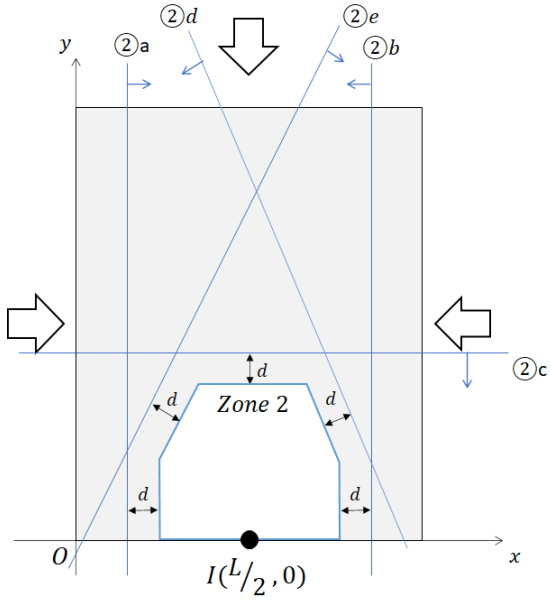

Figure 5.6: Linear inequalities representing Zone 2 with margin $d(>0)$.

We then generate those linear inequalities to represent Zone 2 with the given margin $d(>0)$. The linear inequalities ②a, ②b, ②c, ②d, and ②e (②a- ②e) presented in Figure 5.6 restrict the critical component 1 in S_2 to be located inside Zone 2 with the margin d. The virtual component v_1 is not restricted since it is not an actual component.

When all the critical components are assigned to some zones, we stop the process. Then we collect all those generated constraints ①a-①e and ②a-②e to restrict the locations of the critical components belonging to S_1 and S_2, i.e.,$\{2,3'\}$ and $\{1\}$, respectively. In other words, we add the linear constraints corresponding to ①a-①e, ②a-②e to the proposed MILP model in Section 4.7 and require that components 2 and 3′ satisfy ①a-①e, and the components 1 satisfies ②a-②e. The generated linear constraints for each zone restrict the corresponding critical components only.

Figure 5.7 shows the constraints restricting the corresponding critical components and some possible layouts of the critical components 1,2, and 3′ satisfying the corresponding linear constraints. One of possible layouts of the critical components 1, 2, and 3′ is presented in the exterior hull satisfying the corresponding linear constraints, and some possible layouts of the critical components are provided in Figure 5.7.

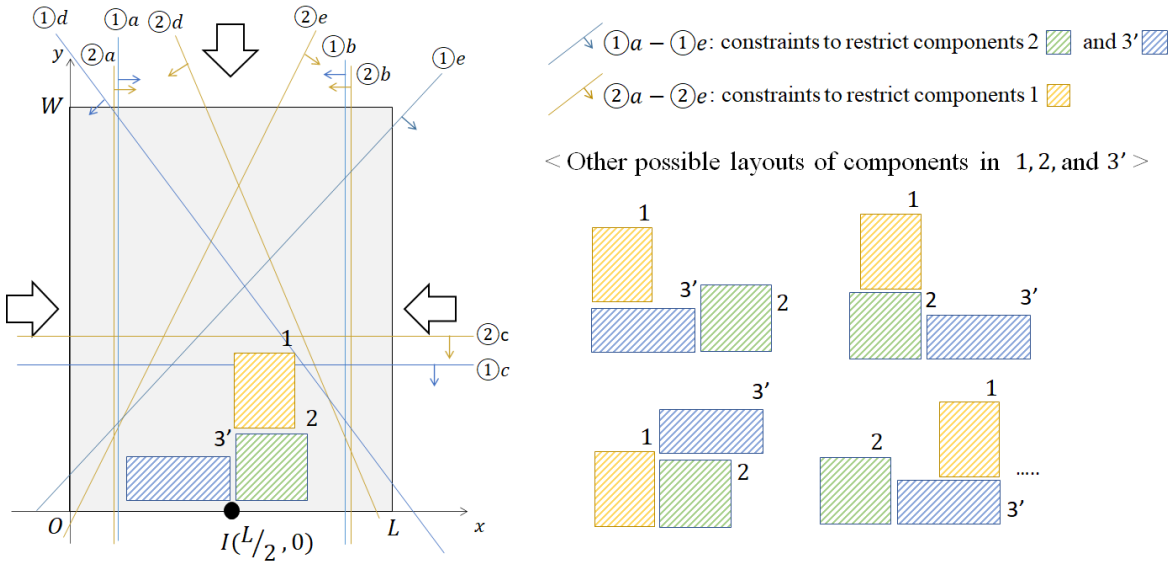

Figure 5.7: Linear constraints for critical components 1,2, and 3′.

Then we add those constraints restricting the corresponding critical components to

the proposed MILP model in Section 4.7, and solve the constraint-added MILP model using a commercial solver.

The above example shows how the zones can be generated to restrict the location of critical components, assuming that the exterior hull is spacious enough to accommodate all the generated zones and the components. In this process, more vulnerable critical components with higher failure probabilities are considered first. We always generate an additional zone to accommodate the next two critical components (if there are more than two left) or the last one and those virtual components accumulated so far. Figure 5.8 illustrates an instance of creating virtual components with 7 critical components, $S_c = \{1,2,3,4,5,6,7\}$ with descending order of failure probabilities $p_i(\forall i \in S_c)$. We first take a set $S_1 = \{1,2\}$ to generate Zone 1. Then the virtual component v_1 is created to represent the critical components 1 and 2 belonging to S_1. Then we take a set $S_2 = \{v_1,3,4\}$ with the virtual component v_1 and critical components 3 and 4 of the next priority to generate Zone 2. Then we have a virtual component v_2 representing the critical components 3 and 4 belonging to S_2. In this way, we can take sets $S_3 = \{v_1, v_2, 5, 6\}$ and $S_4 = \{v_1, v_2, v_3, 7\}$ to generate Zones 3 and 4, respectively. Thus Zone j includes the $j-1$ virtual components derived from Zone 1 to Zone $j-1$. This may help us obtain the proper size of zones. Some linear inequalities are generated to represent the zones with the given margin ($d > 0$), which restrict the locations of the corresponding critical components. Until we have no critical components left to be assigned to any zones, this process is repeated. In the end, we have $\lceil |S_c|/2 \rceil$ zones accommodating the corresponding critical components and virtual components, where $\lceil \ . \rceil$ means the ceiling function.

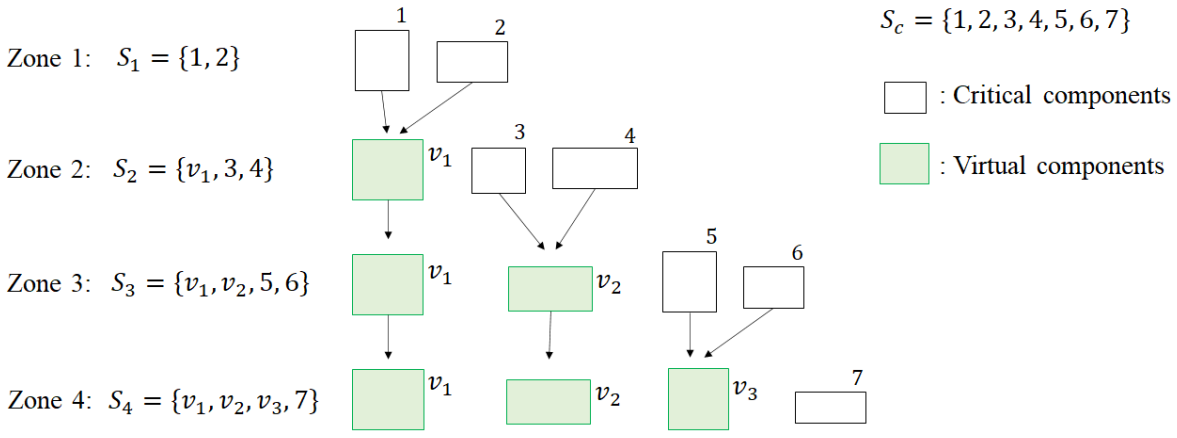

Figure 5.8: Instance of critical and virtual components.

The general procedure of the proposed ZRH method is given below.

Step 0 (Input information) Critical component set S_c, threat directions (θ, ϕ), size (l_i, w_i, h_i) of critical components $(\forall i \in S_c)$, failure probability p_i $(> 0, \forall i \in S_c)$ of critical components, and size of exterior hull (L, W, H).

Step 1 (Initialization) Identify the innermost point I in the exterior hull, which is the location farthest away from the given threat directions (θ, ϕ). Order the critical components in S_c along with the decreasing failure probabilities and keep them in a list L. Virtual component set $S_v \leftarrow \emptyset$ and $j \leftarrow 1$.

Step 2 (Generate Zone j accommodating components in set S_j)

2-1: Add the top two (or the only one left) on the list L to set S_j, and remove them from the list L,

2-2: Add the existing virtual components to S_j, $S_j \leftarrow S_j \cup S_v$,

2-3: Generate a 3D Zone j that can accommodate all possible layouts of the components in S_j, and place the Zone j close to the innermost point I.

Step 3 Generate linear inequalities representing the 3D Zone j with the given margin d to restrict the critical components in S_j only.

Step 4 (Check the remaining critical components) If the list L becomes empty, **MOVE TO Step 5**. Otherwise, create a virtual component v_j with the size of $(l_{v_j}, w_{v_j}, w_{v_j}) \triangleq (\max_{i \in S_j \setminus S_v}\{l_i\}, \max_{i \in S_j \setminus S_v}\{w_i\}, \max_{i \in S_j \setminus S_v}\{h_i\})$. $S_v \leftarrow S_v \cup \{v_j\}$, $j \leftarrow j+1$, and **MOVE TO Step 2** .

Step 5 Add the linear inequalities generated in Step 3, to restrict the corresponding critical components in each S_j only, to the proposed MILP model in Section 4.7. Then solve the constraint-added MILP model using a commercial solver.

In the proposed MILP model in Section 4.7, each grid point requires $(N^2+3N)/2+|S_R|$ binary variables of s_i^k $(\forall i \in S, k \in G)$, $\delta_{i,j}^k$ $(\forall i < j \in S, k \in G)$, and t_i^k $(\forall i \in S \cup \overline{S_c}, k \in G)$, and $2^{|\overline{S_c}|}$ continuous variables of λ_T^k $(\forall T \subseteq \overline{S_c}, k \in G)$. By restricting the locations of critical components to be located in their corresponding zones, a number of the binary variables and continuous variables may be ignored. This enables the ZRH method to generate solutions in a much more efficient manner.

5.2 Computational Experiments

In this section, we first use a practical instance to show the results of adopting the proposed mixed integer linear programming (MILP) model for the optimal component layout of an electric car using both of the commercially available Branch and Cut (B&C) method and the proposed zone-based restriction heuristic (ZRH) method. Then we conduct computational experiments to analyze the performance of the proposed MILP model solved by CPLEX and the proposed ZRH method for optimal layout problems in different sizes.

5.2.1 Optimal Component Layout of Electric Cars

In this subsection, we provide a practical instance to highlight the proposed MILP model for the optimal component layout of an electric car shown in Figure 5.9.

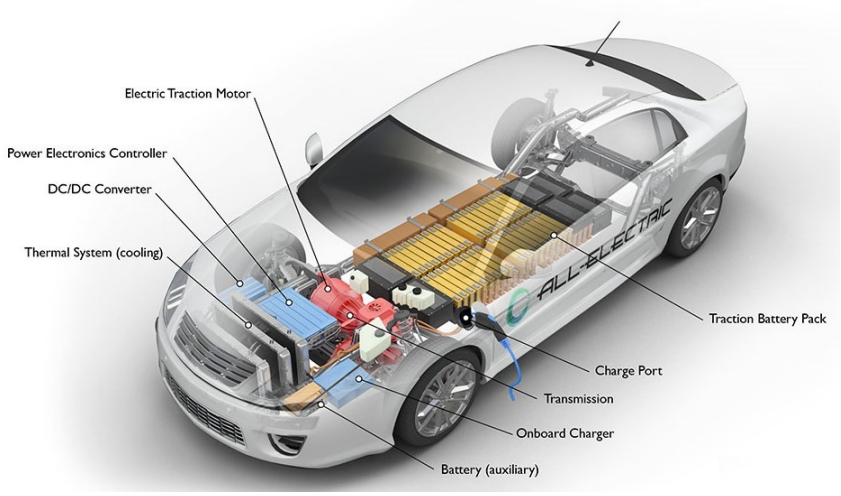

Figure 5.9: Key components in electric cars [DOE].

This electric car includes 7 components: Motor/Transmission (critical component 1), Controller (critical component 2), Converter (critical component 3), Battery Pack (critical component $4'$ with redundancy), Auxiliary Battery (the corresponding redundant component 4 of the critical component $4'$), Onboard charger (non-critical component 5), and Cooling system (non-critical component 6). Thus, we have the component sets $S = \{1,2,3,4',4,5,6\}$, $S_c = \{1,2,3,4'\}$, $S_R = \{4\}$, $S_N = \{5,6\}$. The failure possibilities p_i ($\forall i \in S_c \cup S_R$), the resistance r_i ($\forall i \in S$), and initial penetration capability β_0 are randomly

generated over the sets $\{0.4, 0.5, \ldots, 0.9\}$, $\{10, 15, 20, 25\}$, and $\{15, 18, 21, 24\}$, respectively. The size of the component (l_i, w_i, h_i) is $(15, 15, 15)$, $(10, 10, 15)$, $(10, 15, 15)$, $(10, 10, 10)$, $(10, 10, 10)$, $(15, 15, 10)$, and $(20, 15, 10)$ for the components $1, 2, 3, 4', 4, 5$, and 6, respectively. The size of the exterior hull is $(50, 60, 25)$. The known threat directions are $(\theta, \phi)_1 = (0°, 0°)$ and $(\theta, \phi)_2 = (90°, 0°)$. We chose 80 grid points, i.e., $|G| = 80$, innermost point $I(0, 0, 12.5)$, and margin $d = 5$. Using this information, we solved the proposed MILP model presented in Section 4.7 using both of the commercially available B&C method and the proposed ZRH method.

The instance of the electric car is solved on a computer with the 72 Intel® Xeon Platinum 8352V Processor CPUs @2.1gigahertz and 128gigabyte RAM utilizing ILOG CPLEX 12.8.0. The optimal values, i.e., the maximized weapon survivability ($P_{S/H}$) subjected to a hit, were 0.7406 and 0.7312 from the B&C method and the proposed ZRH method, respectively. The difference of the optimal value was 0.0094, which is less than 1% of weapon survivability. The CPU times for the B&C method and the proposed ZRH were 26.76 minutes and 2.87 minutes, respectively. Figure 5.10 presents the optimal component layouts obtained from the two methods.

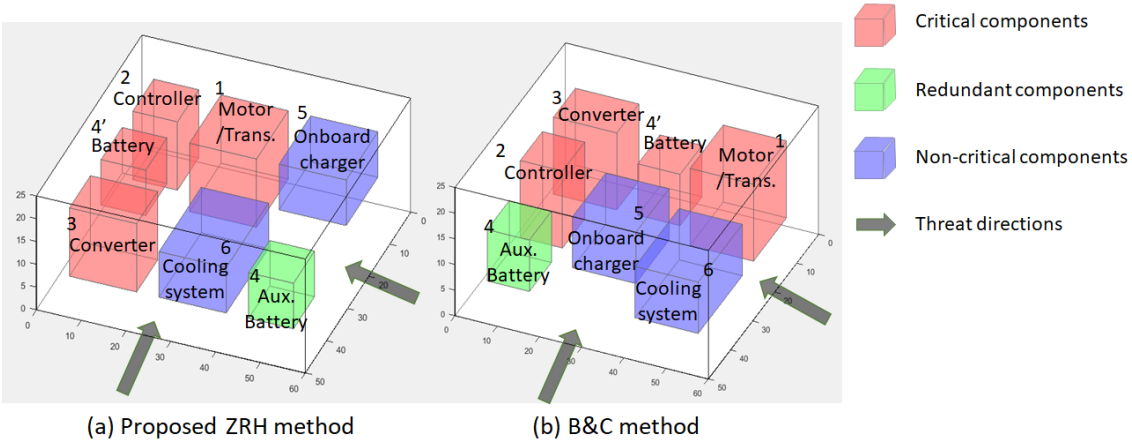

Figure 5.10: Optimal component layouts from the proposed ZRH method and B&C method.

The proposed MILP model takes care of the constraints of feasible layout in the 3D space, adopts the approximated grid point (AGP) approach, also considers the partial penetration and redundant components presented in Sections 4.3, 4.4, 4.5, and 4.6, respectively.

As shown in Figure 5.10, both of the obtained two component layouts are feasible ones in the 3D space.

For adopting the AGP approach, all the components are projected to rectangles since the given threat directions are orthogonal or parallel to the 3D axes. Remember that $s_i^k = 1$ if grid point k is located inside the projected area of component i, otherwise $s_i^k = 0$. Figure 5.11 presents the projected area of the components 1, 3, and 4′ from the threat direction $(0°, 0°)$ of the result obtained by the B&C method. For each grid point k, the binary variable s_i^k is assigned properly as shown in Figure 5.11. For example, in the grid points included by the projected area of the component 3, the variables $(s_1^k, s_3^k, s_{4'}^k)$= $(0, 1, 0)$ since only the projected area of the component 3 includes the corresponding grid point k.

For the concept of partial penetration, the initial penetration capability and the resistance of the components are given as $\beta_0 = 24$ and $(r_1, r_2, r_3, r_{4'}, r_4, r_5, r_6)$=(15, 10, 10, 10, 10, 15, 20), respectively. Figure 5.12 shows the optimal component layout obtained from the B&C method, from two different views.

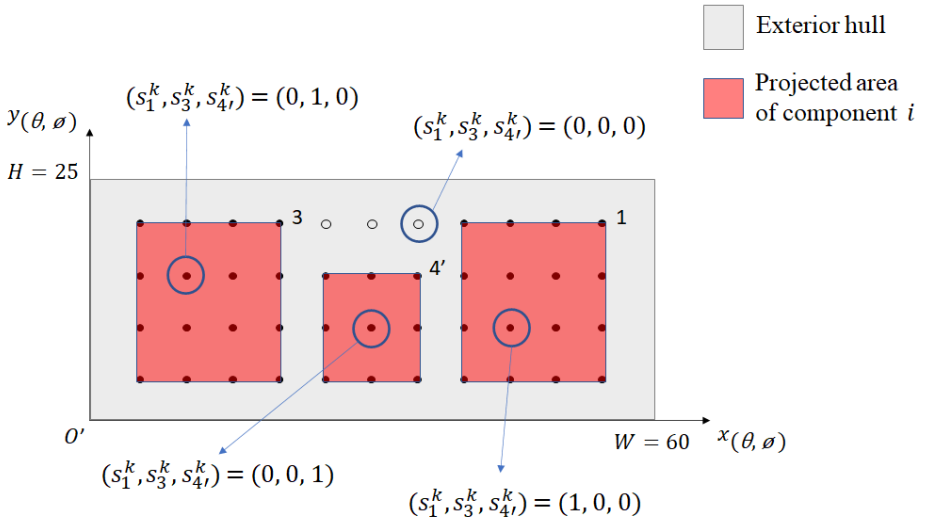

Figure 5.11: Projected areas of components 1, 3, and 4′ from a known threat direction $(0°, 0°)$.

In Figure 5.12 , the three components 2, 3, and 4 are overlapped at the grid point k, i.e, $(s_1^k, s_2^k, s_3^k, s_{4'}^k, s_4^k, s_5^k, s_6^k)$=(0, 1, 1, 0, 1, 0, 0). Notice that $\delta_{i,j}^k = 1$ if component i gets hit before component j at grid point k from a threat direction, otherwise $\delta_{i,j}^k = 0$. Thus, the variables $(\delta_{1,3}^k, \delta_{2,3}^k, \delta_{3,4'}^k, \delta_{3,4}^k, \delta_{3,5}^k, \delta_{3,6}^k)$ should be $(0, 1, 1, 0, 1, 1)$ based on the components' location.

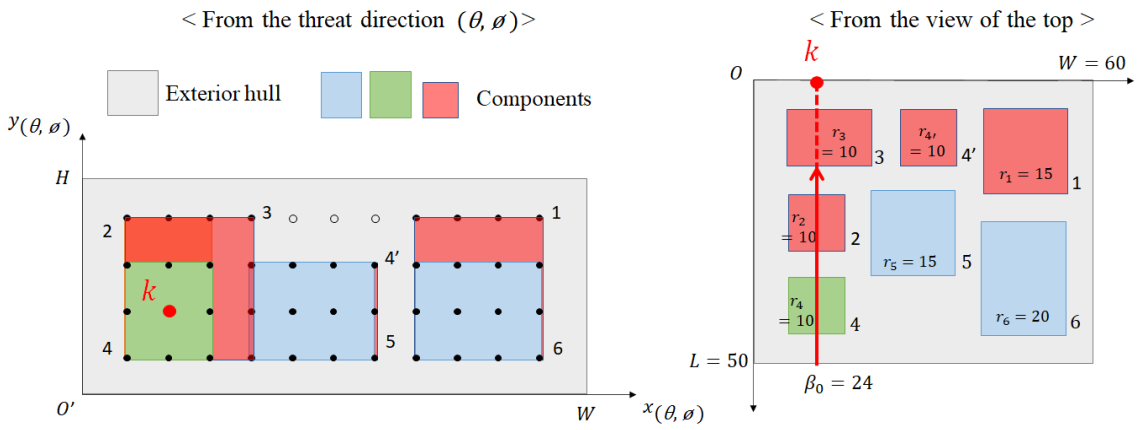

Figure 5.12: Partial penetration in the optimal layout from the B&C method.

Then the residual penetration capacity at grid point k for the component 3 is represented by $\beta_3^k \triangleq \beta_0 - \{r_1\delta_{1,3}^k + r_2\delta_{2,3}^k + r_{4'}(1-\delta_{3,4'}^k) + r_4(1-\delta_{3,4}^k) + r_5(1-\delta_{3,5}^k) + r_6(1-\delta_{3,6}^k)\} = \beta_0 - (r_2 + r_4)$ since $(\delta_{1,3}^k, \delta_{2,3}^k, \delta_{3,4'}^k, \delta_{3,4}^k, \delta_{3,5}^k, \delta_{3,6}^k) = (0,1,1,0,1,1)$. Then, we compare the residual capacity $\beta_3^k (= \beta_0 - (r_2 + r_4) = 4)$ with the resistance of component 3 ($r_3 = 10$) to determine whether t_3^k is one or zero. In this case, t_3^k is forced to be zero since $\beta_3^k < r_3$. Consequently, we have $(t_1^k, t_2^k, t_3^k, t_{4'}^k, t_4^k, t_5^k, t_6^k) = (0,1,0,0,1,0,0)$, which implies only the components 2 and 4 are hit at the grid point k.

Some common features of the two layouts in Figure 5.10 can be observed. First, the critical component (Battery) and its corresponding redundant component (Auxiliary Battery) are laid out apart to prevent being hit together at the same grid point. This is quite reasonable because there is no loss in the weapon survivability unless a critical component and its corresponding redundant component are hit at the same grid point. Second, non-critical components are laid relatively outside of the critical components. Since the non-critical components do not affect the weapon survivability calculation, they could be used to protect critical components. Lastly, critical components are somehow protected by other components as much as possible. In Figure 5.10, most of the critical components are located inside the exterior hull except for Converter (by ZRH) and Motor/transmission (by B&C). These two critical components are inevitably pushed to the outside areas because of the sizes of the exterior hull. In short, critical components are located inside if space allows.

The fundamental difference of the two solutions is that B&C method considers more of the threat direction from $(0°, 0°)$ while ZRH method considers more of threats from the $(90°, 0°)$ direction.

Table 5.1: Parameters in numerical experiments.

	components		(L,W,H)	β_0	(θ,ϕ)	avg. $\lvert G\rvert$
	p_i	l_i, w_i, h_i, r_i				
$N=4$	random value in $\{0.4, 0.5, \ldots, 0.9\}$	random values in $\{5, 10, 15\}$	(40,50,25)	random value in $\{15, 18, 21, 24\}$	$(0°, 0°)$ and $(90°, 0°)$	64
$N=5$	random value in $\{0.4, 0.5, \ldots, 0.9\}$	random values in $\{5, 10, 15, 20, 25\}$	(40,50,25) or (45,50,25)	random value in $\{15, 18, 21, 24\}$	$(0°, 0°)$ and $(90°, 0°)$	70.4
$N=6$	random value in $\{0.4, 0.5, \ldots, 0.9\}$	random values in $\{5, 10, 15, 20, 25\}$	(50,60,25) or (50,65,25)	random value in $\{15, 18, 21, 24\}$	$(0°, 0°)$ and $(90°, 0°)$	76
$N=7$	random value in $\{0.4, 0.5, \ldots, 0.9\}$	random values in $\{10, 15, 20, 25\}$	$L \in \{50, 55\}$ $W \in \{55, 60, 65, 70\}$ $H = 25$	random value in $\{15, 18, 21, 24\}$	$(0°, 0°)$ and $(90°, 0°)$	81.6

5.2.2 Experiment Design

In the rest of this dissertation, all numerical experiments are conducted on a computer with the 72 Intel® Xeon Platinum 8352V Processor CPUs @2.1gigahertz and 128gigabyte RAM utilizing ILOG CPLEX 12.8.0.

We generated 100 instances for each $N = 4, 5, 6$, and 7. Parameters of the instances are shown in Table 5.1. The required information consists of component sets S, S_c, S_R, and S_N, failure possibility p_i ($\forall i \in S_c \cup S_R$), 3-dimensional (3D) size (l_i, w_i, h_i), $\forall i \in S$, resistance r_i ($\forall i \in S$) of components, and 3D size of exterior hulls (L, W, H). Initial penetration capability β_0 and threat directions (θ, ϕ) are also required to describe enemy's threats. Grid point set G is generated based on the 3D size of exterior hull (L, W, H) and the threat directions (θ, ϕ). Notice that the grid point set $G \triangleq \bigcup_{j=1}^{n} G_{(\theta,\phi)_j}$ aggregates the grid point sets $G_{(\theta,\phi)_j}$ generated from all known threat directions $(\theta, \phi)_j$. Moreover, $(|S_c|, |S_R|, |S_N|)$ is set to be $(2,1,1)$, $(3,1,1)$, $(4,1,1)$ or $(4,1,2)$, respectively, for $N = 4, 5, 6$, and 7.

Notice that in Table 5.1, the exterior hull is designed to be spacious enough to accommodate all the generated components. We also generate the grid point set G based on the size of the exterior hull (L, W, H) from each threat direction. We have in general more grid points for larger N values.

5.2.3 Computational Results

In this subsection, we validate the performance of the proposed ZRH method in terms of accuracy and efficiency. To obtain exact optimal solutions, every instance is solved by

the ILOG CPLEX 12.8.0 using the Branch and Cut (B&C) method [Lin11]. When we apply the proposed ZRH method, the constraint-added MILP model in the last step of the ZRH method is also solved in the same environment. We compare and analyze the results from the B&C method and the ZRH method to investigate the performance of the proposed ZRH method.

To validate the accuracy of the proposed ZRH method, we measure the relative optimality gap between the optimal values obtained by the B&C method and the proposed ZRH method, i.e., $(\frac{|z^*_{B\&C} - z^*_{ZRH}|}{z^*_{B\&C}})$. Figure 5.13 plots the average gap of 100 instances for $N = 4, 5, 6,$ and 7.

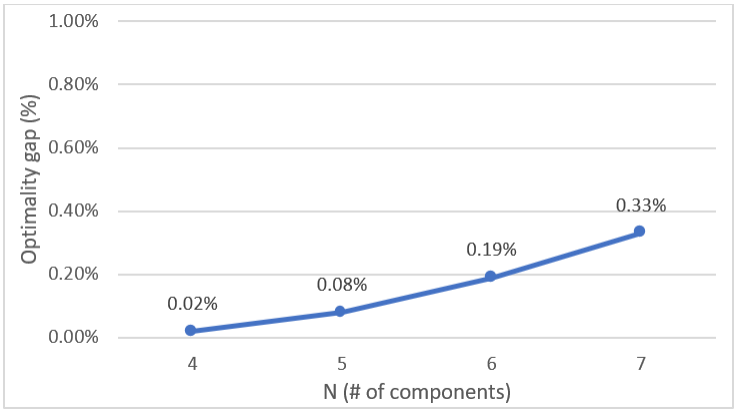

Figure 5.13: Optimality gap on average.

While the gaps are lower than 0.35%, the average gap is slightly increasing as the number of components increases. Nevertheless, the proposed ZRH method performs adequately for problems with up to 7 components to be laid out. We can observe that the ZRH method performs effectively in terms of optimal gaps on average.

Figure 5.14 shows the distributions of optimality gaps for the 100 instances of $N = 4, 5, 6,$ and 7. For $N = 4$, 99 out of 100 instances have good accuracy with less than 1% of the optimality gap. Only one instance has the optimality gap between $[1\%, 2\%)$. The instances of $N = 5$ also show good accuracy with only two instances in the range of $[1\%, 2\%)$ and one instance in the range of $[2\%, 3\%)$. The gaps become to widen as the number of components increases, as expected. Overall speaking, the ZRH method is capable of providing high quality solutions to the proposed MILP model.

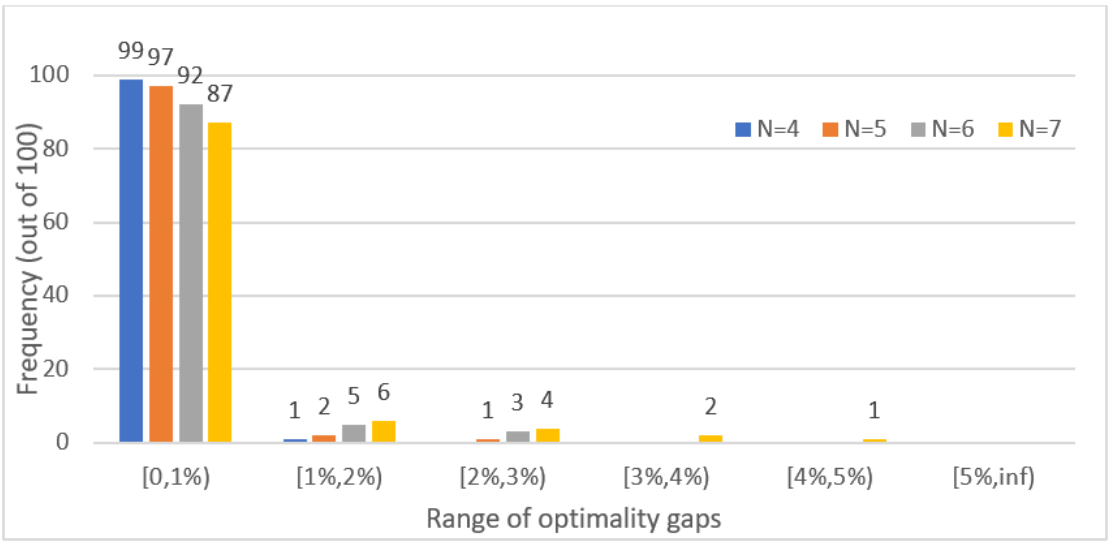

Figure 5.14: Optimality gap distribution.

Figure 5.15 shows the average CPU times of the B&C method and ZRH method for $N = 4, 5, 6$, and 7. The improvement (%) is defined to be (B&C time - ZRH time)/(B&C time).

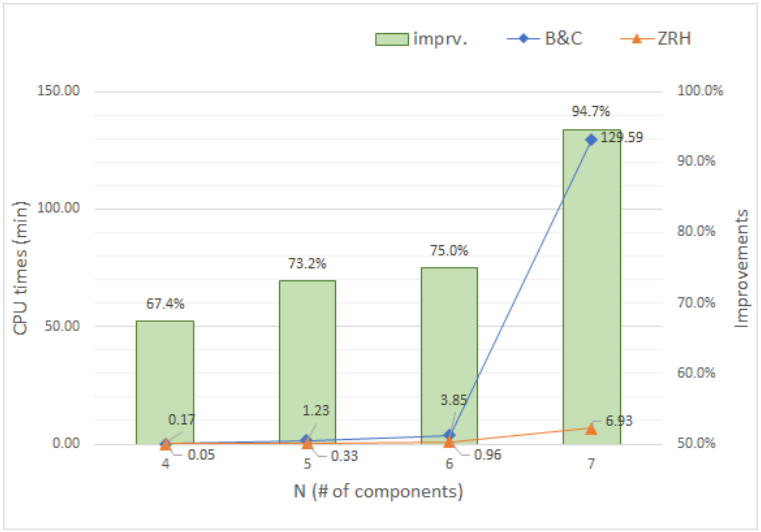

Figure 5.15: Runtime performance on average.

Table 5.2: Runtime performance.

Method	CPU time (min)			
	$N=4$	$N=5$	$N=6$	$N=7$
	mean/std	mean/std	mean/std	mean/std
ZRH	0.054/0.040	0.330/0.218	0.964/0.760	6.931/5.689
B&C	0.166/0.115	1.230/0.934	3.855/2.761	129.591/158.980

The average and standard deviations (std) of CPU times from the proposed ZRH method and B&C method are also included in Table 5.2. It can be easily observed from Figure 5.15 and Table 5.2 that the ZRH method runs faster than the B&C method in all cases. Moreover, the running time of the ZRH method grows slowly contrasting to the sharp spike of the B&C method from $N=6$ to $N=7$.

Overall speaking, we can confirm that the ZRH method can provide high quality solutions to the proposed MILP model in an efficient manner. Moreover, it holds good potential for solving problems with a large number of components involved in a weapon system.

CHAPTER

6

CONCLUDING REMARKS

6.1 Summary of Dissertation

In this thesis, we have proposed a novel approximated grid point (AGP) approach to model the vulnerability of weapon systems. Based on this approach, we can easily manage the shape of the projected area of each component and realize the concept of weapon vulnerability into a mathematical model. We have first formulated the problem into a mixed integer nonlinear programming (MINLP) model including all types of components and the concepts of partial penetration and component redundancy. Then we converted the MINLP model into a mixed integer linear programming (MILP) model using the concept of pseudo-Boolean expressions for computational efficiency. In addition, a zone-based restriction heuristic (ZRH) method has been proposed to generate high quality solutions of large-scale component layout problems in a much more efficient manner.

Chapter 3 mainly studies the assessment approach of the weapon vulnerability. As preliminaries, we provide some basic concepts including threat directions, parallel projections, and geometry of cuboids. These concepts are used to assess the weapon vulnerability and to formulate our mathematical model in Chapter 4. Then the vulnerable area (VA)

approach is introduced with simple examples to clearly explain its mechanism with its limitation to be adopted in mathematical models. We also propose an approximated grid point (AGP) approach, which is evolved from the VA approach. Using the same examples, we discuss the difference between the two approaches and show some advantages of the proposed AGP approach.

Chapter 4 provides a mathematical model for the minimal vulnerability of weapon systems. We provide the problem statement and notations used for the proposed mathematical model. The optimization model includes all types of components and reflects some realistic constraints such as feasibility in the 3D space, partial penetrations, and component redundancy. We formulate the problem as an MINLP model first and convert it to an MILP model by a linearization mechanism using the concept of pseudo-Boolean expressions.

Chapter 5 presents the "zone-based restriction heuristic" method to solve the proposed MILP in a much more efficient manner. Although we can solve the proposed MILP model using commercial solvers, low computation efficiency can be caused by a large number of binary variables and constraints. The low computational efficiency may be a critical issue in attaining the optimum of the proposed MILP model. The proposed heuristic method is designed by considering component's characteristics for priority to protect. Based on this idea, we improve computational efficiency by restricting the locations of critical components. Then we present a practical instance to validate the proposed MILP model for the optimal component layout using both of the commercially available Branch and Cut (B&C) method and proposed ZRH method. Then computational experiments are provided to analyze the performance of the proposed proposed ZRH method in different sizes, in terms of accuracy and efficiency.

6.2 Future research

Following this study, we may improve the computational accuracy of solving the proposed MILP model and expand the current model to a more advanced one adopting complicated issues such as repetitive hits and multi-kill modes of weapon systems.

The concept of warm starting may be effective to obtain more accurate solutions to the proposed MILP model. We verified the performance of the proposed ZRH method, and its solutions can be used as good starting points to lead to much more accurate optimal solutions. Instead, the trade-off between accuracy and efficiency will be inevitable.

Some ideas for the multiple hits are introduced in [Bal03]: the binomial approach for

N hits, Poisson process for E expected hits, tree diagram, and Markov chain. In particular, the binomial approach exactly calculates the probability from N hits and Poisson process computes the expected number of hits (E) when weapon systems are hit for N times. We can also list all the possible cases given N hits using a tree diagram. Additionally, we can model the Markov chain using a transition matrix of states of disabled components.

Moreover, after learning how to obtain optimal component layouts for each of the multi-kill modes of weapon systems, we may simply optimize a weighted sum of the vulnerabilities for the problem with multiple kill modes. It is also possible to apply the concept of Pareto optimum [Alh04] to study the problem. Bi-level optimization could be a suitable model to obtain the optimal component layout of a weapon system subject to two kill modes.

REFERENCES

[Alh04] Alhammadi, H. Y. and Romagnoli, J. A. Chapter B4 of The Integration of Process Design and Control, edited by P. Seferlis and M. C. Georgiadis, in Process design and operation incorporating environmental, profitability, heat integration and controllability considerations. *Computer Aided Chemical Engineering*, 17:264–305, 2004.

[Arn69] Arnold, R. J. Survivability design of forward air control and light attack aircraft. *Society of Automotive Engineers*, (SAE Paper 690707), 1969.

[Atk69] Atkinson, D. B., Blatt, P., Mahood, L., and Voyls, D. W. Design of fighter aircraft for combat survivability. *Society of Automotive Engineers*, (SAE Paper 690706), 1969.

[Bal94] Ball, R. E. and Calvano, C. N. Establishing the fundamentals of a surface ship survivability design discipline. *Navy Engineers Journal*, 106(1):71–74, 1994.

[Bal98] Ball, R. E. and Atkinson, D. B. A history of the survivability design of military aircraft. *Report #ADA351434, Naval Postgraduate School Monterey CA*, pages 75–89, 1998.

[Bal03] R. E. Ball. *The Fundamentals of Aircraft Combat Survivability Analysis and Design, Second Edition*. American Institute of Aeronautics and Astronautics, 2003.

[Bar02] Barbosa-Povoa, A. P., Mateus, R., and Novais, A. Q. Optimal 3D layout of industrial facilities. *International Journal Production Research*, 40(7):1669–1698, 2002.

[Cra93] Yves Crama. Concave extensions for nonlinear 0-1 maximization problems. *Mathematical Programming*, 61:53–60, 1993.

[D'A17] D'Ambrosioa, C., Nannicini, G. and Sartor, G. MILP models for the selection of a small set of well-distributed points. *Operations Research Letters*, 45:46–52, 2017.

[DOE] DOE, U. S. department of Energy. How do all-electric cars work? https://afdc.energy.gov/vehicles/how-do-all-electric-cars-work. Online; accessed 1-October-2021.

[Dri13] M. R. Driels. *Weaponeering: Conventional Weapon System Effectiveness*. American Institute of Aeronautics and Astronautics, 2013.

[DSI] DSIAC, Defense Systems Information Analysis Center. Vulnerability toolkit from defense systems information analysis Center. https://www.dsiac.org/resources/models-and-tools/vulnerability-toolkit. Online; accessed 1-March-2020.

[Fal76] Falk, J. E. and Hoffman, K. R. A successive underestimation method for concave minimization problems. *Mathematics of Operations Research*, 1:251–259, 1976.

[Flo95] C. A. Floudas. *Nonlinear and Mixed-Integer Optimization.* Oxford University Press, 1995.

[Har10] Harney, R. C. Broadening the trade space in designing for warship survivability. *Navy Engineers Journal*, 122(1):49–63, 2010.

[Hen82] G. B. Hendon. Aircraft survivability equipment from the lab to the field. *Journal of Electronics Defense*, April:46–53, 1982.

[Her91] Heragu, S. S. and Kusiak, A. Efficient models for the facility layout problem. *European Journal of Operational Research*, 53:1–13, 1991.

[ILO] ILOG CPLEX Optimization Studio. Solving mixed integer programming (MIP) problems. https://www.ibm.com/docs/en/icos/12.7.1.0?topic=optimization-solving-mixed-integer-programming-problems-mip. Online; accessed 1-October-2021.

[Jab65] E. Jablonski. *Flying Fortress.* Garden City, N.Y., Doubleday, 1965.

[JC58] R. S. Johnson and M. Caidin. *Thunderbolt.* New York, Rinehart, 1958.

[Jee18] Jee, Y., Kim, T., and Hong, S.-P. Component layout for minimizing weapon vulnerability using mixed integer programming. *Journal of the Korean Operations Research and Management Science*, 43(2):55–64, 2018.

[Jee19] Y. Jee. Component layout of combat vehicle for minimizing vulnerability. *Master Thesis. Department of Industrial Engineering, Seoul National University, South Korea*, 2019.

[Ji 19] Ji , B., Yuan, X., Yuan Y., Lei, X., Fernando, T., and Iu, H. Exact and heuristic methods for optimizing lock-quay system in inland waterway. *European Journal of Operations Research*, 277:740–755, 2019.

[Kol18] Kolanowska, A., Janasa, D., Herman A. P., Jędrysiak R. G., Giżewski, T., and Boncel, S. From blackness to invisibility – carbon nanotubes role in the attenuation of and shielding from radio waves for stealth technology. *Carbon*, 126:31–52, 2018.

[Lin11] Linderoth, J. T. and Lodi, A. MILP software. *Wiley Encyclopedia of Operations Research and Management Science*, 5:3239–3248, 2011.

[Mer16] Merrell, T. T. Gaining through training: pilot proficiency in modern combat aviation. *Accession Number: AD1030450, Defense Technical Information Center*, 2016.

[NRC93] NRC, National Research Council. *Vulnerability Assessment of Aircraft: A Review of the Department of Defense Live Fire Test and Evaluation Program.* Washington, DC: The National Academies Press, 1993.

[Qin17] Qin, Z. and Liang, Y. G. Layout optimization of satellite cabin considering space debris impact risk. *Journal of Spacecraft and Rockets*, 54(5):1176–1180, 2017.

[Qin18] Qin, Z., and Liang, Y. G. Multiobjective methodology for satellite cabin layout optimization considering space debris impact risk. *Optimization and Engineering*, 55(1):232–235, 2018.

[Rem76] R. T. Remers. Design for reduction of aircraft vulnerability. *Proceedings on Aircraft Operational Experience and Its Impact on Safety and Survivability*, 212:19–1–19–23, 1976.

[Roc70] R. T. Rockafellar. *Convex Analysis*. Princeton University Press, 1970.

[Sch13] Schwing, A. G., Fidler, S., Pollefeys, M., and Urtasun, R. Box in the box: joint 3D layout and object reasoning from single images. *2013 IEEE International Conference on Computer Vision*, pages 353–360, 2013.

[Vav91] S. A. Vavasis. *Nonlinear Optimization: Complexity Issues*. Oxford University Press, 1991.

[Wan19] Wang, S., Lan, L., Liu, Y., Tang, M., and Wen, M. Effects of local coating on strengthening and crack suppression of notched PBX beams. *Propellants, Explosives, Pyrotechnics*, 44:1361–1367, 2019.

[Wol98] L. A. Wolsey. *Integer Programming*. Wiley, 1998.

[Yi,14] Yi, K. J., Baek, S. W., Kim, M. Y., Lee, S. N., and Kim, W. C. The effects of heat shielding in jet engine exhaust systems on aircraft survivability. *International Journal of Computation and Methodology*, 66(1):89–106, 2014.

[Zho19] Zhong, C.-Q., Xu, Z.-Z. and Teng, H.-F. Multi-module satellite component assignment and layout optimization. *Applied Soft Computing Journal*, 75:148–161, 2019.